

# Mineral Chemistry and Pressure–Temperature Evolution of Two Contrasting High-pressure–Low-temperature Belts in the Chonos Archipelago, Southern Chile

ARNE P. WILLNER<sup>1\*</sup>, FRANCISCO HERVÉ<sup>2</sup> AND HANS-JOACHIM MASSONNE<sup>3</sup>

<sup>1</sup>INSTITUT FÜR MINERALOGIE, RUHR-UNIVERSITÄT, D-44780 BOCHUM, GERMANY

<sup>2</sup>DEPARTAMENTO DE GEOLOGIA, UNIVERSIDAD DE CHILE, CASILLA 13518, CORREO 21, SANTIAGO DE CHILE, CHILE

<sup>3</sup>INSTITUT FÜR MINERALOGIE UND KRISTALLCHEMIE, UNIVERSITÄT STUTT GART, AZENBERGSTR. 18, D-70174 STUTT GART, GERMANY

RECEIVED OCTOBER 29, 1998; REVISED TYPESCRIPT ACCEPTED SEPTEMBER 9, 1999

*The Chonos Metamorphic Complex forms part of a belt of low-grade metamorphic rocks in the Chilean Coastal Cordillera that are interpreted as Palaeozoic–Mesozoic accretionary complexes. It comprises metapsammopelitic schists, metabasites and meta-ironstones occurring in two contrasting units. Special attention during microprobe study of key samples was given to the chemical zonation of minerals. Subsequently, conventional geothermobarometry and that using thermodynamic calculations were applied. The Eastern belt comprises rocks that are metamorphosed to pumpellyite–actinolite facies conditions and show a low degree of deformation with well-preserved sedimentary and igneous structures. Maximum P–T conditions were around 5.5 kbar and 250–280°C. The rocks of the Western belt are characterized by a transition between greenschist and albite–epidote–amphibolite facies metamorphism and show a penetrative tectonic transposition foliation  $S_2$  formed close to the pressure maximum. Maximum P–T conditions vary around 8–10 kbar and 380–500°C overstepping the stilpnomelane + phengite stability. High pressures in this belt are confirmed by regionally distributed phengites with high Si contents up to 3.5 Si per formula unit. Regional distribution of maximum temperatures is reflected by the composition of actinolitic hornblendes within the metabasites. In a garnet-bearing metabasite of the Western belt, oscillatory growth zoning of garnet was observed. The composition of corresponding mineral inclusions suggests that a prograde P–T path during garnet growth evolved from 7.5 kbar and 375°C to about 9.4 kbar and 500°C. Late garnet grew synkinematically with*

*penetrative deformation. The retrograde P–T path in the rocks of the Western belt is constrained by the composition of mainly late strain-free minerals and involves slight cooling during decompression. Both belts are part of a subduction system. The apparent P–T gap between the belts is due to their juxtaposition during exhumation. The Eastern belt constitutes the transition towards the backstop system of the accretionary prism that is represented by the Western belt, whereas the absence of very low grade rocks west of the Western belt is attributed to tectonic erosion, which was possibly caused by subduction of a ridge.*

KEY WORDS: Chonos Metamorphic Complex; accretionary complex; high-pressure–low-temperature metamorphism; oscillatory garnet zonation; phengite; P–T paths

## INTRODUCTION

The Chonos Archipelago (latitude 44°–46°S; Fig. 1a) of Southern Chile is mainly composed of low-grade metamorphic rocks, which constitute a great part of the present Chilean Coastal Cordillera between 32°S and 54°S, forming an almost continuous belt (Fig. 1b). This belt is considered to represent accretionary complexes

\*Corresponding author. e-mail: arne.willner@ruhr-uni-bochum.de

developed at the southwestern margin of Gondwana during the Late Palaeozoic and Mesozoic with ages of metamorphism decreasing towards the south (Hervé, 1988). The low-grade metamorphic rock suite contains rare local occurrences of blueschists, but the HP–LT nature of the suite is evidenced by abundant phengites, relatively rich in Si, in widespread metapsammopelitic rocks and intercalated metabasites (Massonne *et al.*, 1996). This contrasts with the metamorphic rocks north of 32°S, where no HP–LT rocks have been described until the present. A contemporaneous Upper Palaeozoic magmatic arc and related LP–MT to LP–HT metamorphic rocks exist only in the northern part of the belt at the eastern side of the low-grade belt (Aguirre *et al.*, 1972), whereas in the middle and southern part intrusion of calc-alkaline plutonites of the Mesozoic Patagonian batholith into the low-grade belt occurred later (Hervé, 1988). At present, the Southern Volcanic Zone of the Andes runs parallel to the low-grade belt in the east, as does a small recent sedimentary accretionary wedge in the west (Bangs & Cande, 1997). The present situation is characterized by oblique subduction of the Nazca plate, which has caused a dextral strike-slip structure controlling the emplacement of the active volcanic belt (Cembrano *et al.*, 1996). The long hiatus in the accretion history and the apparent rarity of HP–LT belts along the entire Andean convergent margin is striking.

The lithological characteristics, structure and age of the Chonos Metamorphic Complex (CMC) have been described in some detail by Miller (1979), Hervé *et al.* (1981, 1988), Godoy *et al.* (1984) and Davidson *et al.* (1987). According to these workers the complex is constituted by (1) an Eastern belt composed of submarine fan turbidite sequences and subordinate pelagic metacherts as well as very rare greenschists, both with well-preserved primary structures, and (2) a Western belt, mainly formed by strongly foliated and tectonically transposed mica schists and greenschists with occasional metacherts and meta-ironstones. Primary premetamorphic structures are lacking in the latter belt. Blue amphiboles have been found at only two localities so far in the CMC, by Davidson *et al.* (1987). This specific subdivision is characteristic for most of the occurrences in the Chilean Coastal Cordillera, but is particularly well exposed in the Chonos Archipelago (Hervé, 1988).

As a result of new fossil findings, it is considered that sedimentation in the Eastern belt persisted to Late Triassic times (Fang *et al.*, 1998). This was corroborated by U/Pb ages of detrital zircons of 220–240 Ma from the fossil locality determined by Hervé (1998). The ages of metamorphism and the related generation of the ductile deformation structures are so far only approximately known by Rb–Sr errorchrons. They cluster at 253–263, 215–223 and 135–168 Ma (Davidson *et al.*, 1987; Hervé *et al.*, 1988). The latter clusters are confirmed

by K–Ar whole-rock ages in two intervals at 208–223 and 133–188 Ma (Garrido, 1987; Hervé *et al.*, 1988). Davidson *et al.* (1987) supposed a probable formation of an accretionary prism as early as Permian–Triassic and a later deformational–metamorphic event during Jurassic–Cretaceous times, because there is a tendency towards younger ages in rocks with stronger deformational imprint and higher metamorphic grade in the Western belt. The dating of metamorphism deserves more detailed work, for dating of minerals formed during a specific deformation episode under defined *P–T* conditions.

The CMC was later intruded by calcalkaline plutons of the North Patagonian batholith: the Eastern belt is bounded to the east by Early Cretaceous plutons in its southern portion (K–Ar hornblende ages of 145 Ma and biotite ages of 121–138 Ma as well as Rb–Sr isochron ages of 125–140 Ma; Godoy *et al.*, 1984; Davidson *et al.*, 1987; Pankhurst & Hervé, 1994) and by an Eocene pluton in its northern part (Pankhurst & Hervé, 1994). A Late Cretaceous satellite intrusion (K–Ar biotite ages of 67–75 Ma, Rb–Sr biotite as well as whole-rock ages of 48–76 Ma; Godoy *et al.*, 1984; Hervé *et al.*, 1997) intrudes the Western belt in the southwestern part (Fig. 1). All these plutons are intrusions with small contact metamorphic haloes containing biotite, cordierite or andalusite. These low-pressure assemblages suggest that uplift of the deeply buried metamorphic rocks was almost completed by the time of plutonic intrusion.

The most striking feature within the CMC (and hence for most occurrences along the Chilean Coastal Cordillera) is the occurrence of lower-grade metamorphic rocks (the Eastern belt) to the east of the low-grade Western belt. This type of metamorphic zonation seems to contradict the classic concept proposed by Ernst (1975) for fossil circum-Pacific accretionary prisms, where metamorphic grade and age increase away from the trench, marking a subduction polarity. However, subduction along the South American convergent margin can generally be assumed to have occurred from western directions during the Mesozoic and Cenozoic, and this is confirmed by the generally NE-dipping foliation planes in the CMC (Davidson *et al.*, 1987). Hence a problem arises concerning the meaning of a lower-grade zone to the east of the Western belt.

The purpose of this paper is to present new quantitative chemical data on metamorphic minerals of representative rock types of the Chonos Archipelago, applying new geothermobarometric techniques. These data allow a quantitative characterization of the *P–T* conditions of the metamorphic evolution of the complex, which previously have been only qualitatively described as low-grade metamorphism, transitional from greenschist to blueschist facies (Davidson *et al.*, 1987). In addition, we aim to contribute to solutions of the

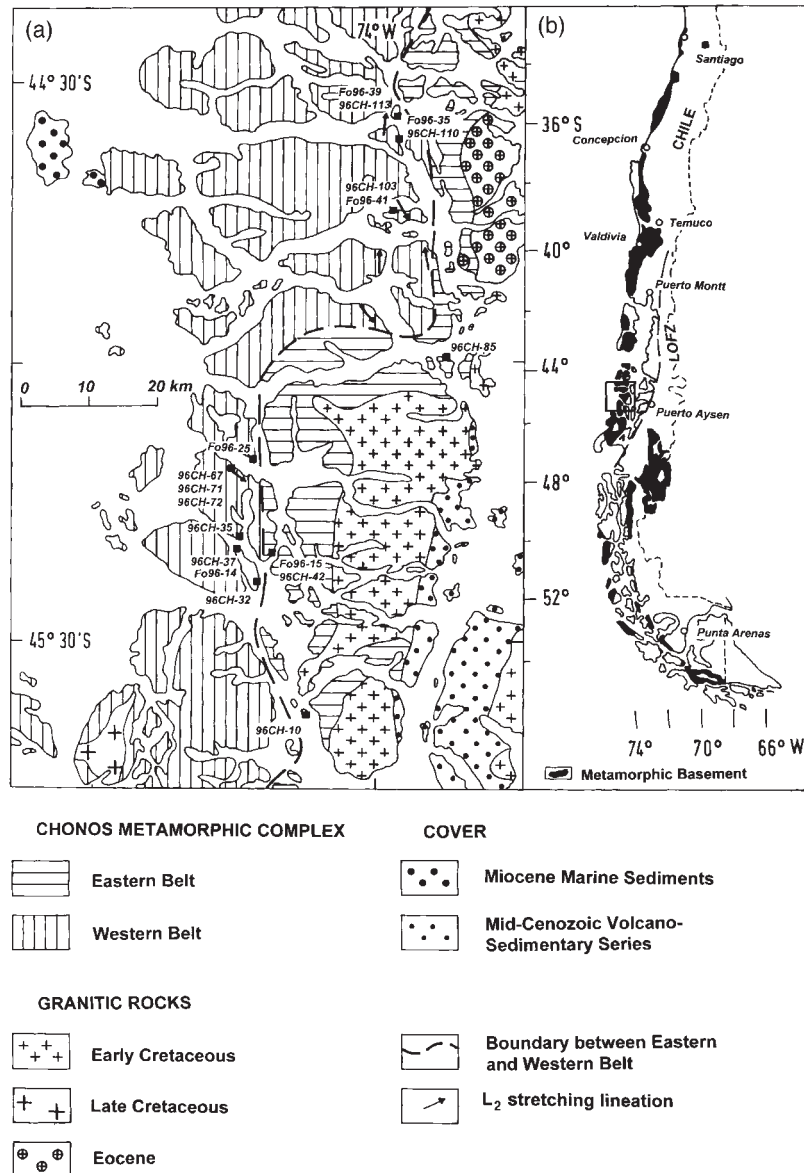


**Fig. 1.** (a) Location map of studied samples in the Chonos Archipelago. Geology after Davidson *et al.* (1987). (b) Insert map: distribution of Late Palaeozoic-Mesozoic metamorphic basement (black; undifferentiated; predominantly low grade) in the Southern Andes; LOFZ, Liqueñe Ofqui Fault Zone; the location of map (a) in the Chonos Archipelago is marked.

following problems related to the origin of accretionary wedges in general:

(1) which indications of HP-LT metamorphism may exist apart from the presence of blueschists, and how widespread are they?

(2) Can partial *P-T* paths be established, which are characteristic for a specific type of subduction complex? What information is actually preserved in the rocks?

(3) Are the two belts of the CMC structurally coherent? What parts of a subduction system do they represent?

## FIELD RELATIONSHIPS, PETROGRAPHY AND MINERAL CHEMISTRY

The study concentrated on three groups of lithologies: metapsammopelitic schist, metabasite, and meta-ironstone and metachert. The last two rock types are generally associated with the metabasite. The locations of samples with mineral compositions studied in detail are indicated in Fig. 1a. A synthesis of their petrographical characteristics and mineral chemistry, in particular, is given

below. Because rather monotonous metapsammopelitic schists dominate by far and intercalations of other rock types are rare, sampling along systematic cross-sections that are also spread over many islands is difficult. Nevertheless, we were lucky that most key samples were located fairly close to the boundary between the two belts. Unfortunately, we were not able to resample and study blueschists (Davidson *et al.*, 1987) during the field campaign related to this work.

### Analytical methods

The mineral analyses were obtained with a Cameca SX 50 microprobe at Ruhr-Universität Bochum, and a Jeol Superprobe (JXA-8600MX) at the Johannes-Gutenberg-Universität, Mainz. Operating conditions were an acceleration voltage of 15 kV, a beam current of 15 nA, 20 s counting time per element and a slightly defocused beam of 5  $\mu\text{m}$  to avoid loss of alkalis. Standards used were the following (those of Mainz are given in parentheses): synthetic pyrope (wollastonite) for Si, synthetic pyrope (corundum) for Al, rutile ( $\text{MnTiO}_3$ ) for Ti, glass of andradite composition (haematite) for Fe, synthetic pyrope ( $\text{MgO}$ ) for Mg, glass of andradite composition (wollastonite) for Ca, jadeite (albite) for Na, K-bearing glass (orthoclase) for K, NaCl (tugtupite) for Cl, topaz (F-phlogopite) for F,  $\text{Cr}_2\text{O}_3$  for Cr, Ba-silicate glass (baryte) for Ba ( $\text{La}$ ). The PAP procedure was used for matrix correction. Representative analyses and structural formulae of minerals used for calculations are presented in Tables 1–5, including the calculation procedure. Further analyses can be provided upon request by the first author. Element distribution maps for three elements were simultaneously produced by stepwise scanning over rectangular areas using a Camebax microprobe in Bochum.

### The Eastern belt

Within most of the Eastern belt, submarine fan turbidite sequences occur with alternating slates and sandstones in stratal continuity and with well-preserved primary sedimentary structures. These are deformed by tight chevron folds that are mainly NNW-trending and overturned to the SW with wavelength up to several tens of metres and a penetrative axial plane cleavage  $S_1$  (Davidson *et al.*, 1987). These are locally cut by 0.5–4 km wide zones of 'broken formations' with disrupted and isolated sandstone blocks of metre size rotated in a matrix of dark slates with a penetrative  $S_1$  cleavage. These are interpreted as cataclastic melange-type shear zones (Garrido, 1985; Hormazábal, 1991) subparallel to the axial planes of the  $F_1$  folds. Locally, metacherts and more rarely metabasites, also internally showing well-preserved primary magmatic fabrics, are tectonically interleaved.

Locally, a flat to gently NE-dipping  $S_2$  crenulation cleavage is developed.

### Massive metabasites of the Eastern belt

The best-exposed occurrence of metabasites of the Eastern belt is a small belt of isolated lensoid bodies on Isla Dring and Isla Italia, which were well studied by Hervé *et al.* (1994). To the west these are in contact with coherent turbidite sequences showing well-preserved bedding planes, but to the east they are in contact with melange bodies. All contacts of the metabasite lenses are of tectonic nature. The metabasites are massive rocks with a heterogeneous development of a crude anastomosing foliation mainly near the contacts of the lenses. Partly pillow structures are preserved and a chemical composition resembling P-type mid-ocean ridge basalts (MORBs) (Hervé *et al.*, 1994).

Samples F96-15 and 96CH-42 were collected in the central part of a lens of several hundred metres thickness on the southern shores of Isla Dring ( $45^\circ 21.4'S$ ,  $74^\circ 12.8'W$ ). These rocks maintained their original subophitic texture with relic phenocrysts. Most conspicuous is augite with notable  $\text{TiO}_2$  contents (0.71–1.36 wt %; Table 1). According to Hervé *et al.* (1994), its composition is characteristic for alkali basalts. Further presumable relic phenocrysts are isolated clusters of plagioclase (now albite) up to 1 mm in size in a very fine-grained non-oriented matrix.

The metamorphic mineral assemblage is albite–quartz–amphibole–pumpellyite–I–chlorite–stilpnomelane–titanite. The rock is cut by a system of veinlets composed mainly of white mica. The veinlets develop rims 0.4 mm wide, which appear to replace the matrix and are composed of coarser grains of albite + pumpellyite II + amphibole + chlorite. Stilpnomelane appears in isolated radial aggregates. Epidote is present, but was not observed in mutual contact with amphibole. In addition, the rock contains fissures filled by pyrite and chalcocopyrite, and more rarely calcite.

The white mica in the veinlets is phengite showing a systematic compositional zoning with increasing Si contents from 3.4 to 3.5 p.f.u. (per formula unit) and  $X_{\text{Mg}}$  [ $\text{Mg}/(\text{Mg} + \text{Fe}^{2+})$ ] from 0.2 to 0.6 from core to rim (Table 4). Na and Ti contents are close to the detection limit. Amphibole does not show significant variation in matrix and veinlets, being actinolite with  $X_{\text{Mg}}$  around 0.52 (Table 3). However, pumpellyite exhibits considerable differences between matrix and veinlets, suggesting that they represent two generations: the matrix grains have  $X_{\text{Mg}}$  of 0.4–0.6 and  $X_{\text{Fe}^{3+}}$  [ $\text{Fe}^{3+}/(\text{Fe}^{3+} + \text{Fe}^{2+})$ ] of 0.3–0.5, whereas those in the vein margins have  $X_{\text{Mg}}$  around 0.1 and  $X_{\text{Fe}^{3+}}$  of 0.02 (Table 2). Chlorite shows a rather uniform composition with  $X_{\text{Mg}}$  around 0.4, Si contents around 5.8 p.f.u. and Mn contents

Table 1: Representative analyses of garnet and clinopyroxene

	Garnet						Clinopyroxene	
	96CH-113				96CH-72		Fo96-15	
	I	II	III	IV	Core	Rim		
SiO <sub>2</sub>	37.27	36.97	37.53	37.86	36.13	37.16	SiO <sub>2</sub>	50.42
TiO <sub>2</sub>	0.27	0.16	0.07	0.15	0.52	0.13	TiO <sub>2</sub>	0.71
Al <sub>2</sub> O <sub>3</sub>	20.27	20.97	20.95	20.69	14.25	20.24	Al <sub>2</sub> O <sub>3</sub>	3.52
Fe <sub>2</sub> O <sub>3</sub> *	0.93	0.63	0.94	0.91	9.20	0.86	Cr <sub>2</sub> O <sub>3</sub>	0.14
FeO	21.37	26.95	27.73	29.63	6.37	20.92	Fe <sub>2</sub> O <sub>3</sub> *	1.47
MnO	8.28	3.30	1.23	0.71	28.62	13.61	FeO	6.93
MgO	0.50	1.41	1.07	1.71	0.03	0.30	MnO	0.21
CaO	11.13	9.38	11.20	9.67	5.90	6.46	MgO	14.74
Sum	100.02	99.77	100.72	101.33	100.02	99.68	Na <sub>2</sub> O	0.25
							CaO	20.57
Si	5.953	5.936	5.959	6.007	5.996	6.037	Sum	98.96
Al <sup>IV</sup>	0.047	0.064	0.041	0.000	0.004	0.000		
Sum	6.000	6.000	6.000	6.000	6.000	6.000	Si	1.889
							Al <sup>IV</sup>	0.111
Al <sup>VI</sup>	3.853	3.905	3.879	3.869	2.784	3.875	Sum	2.000
Fe <sup>3+</sup>	0.113	0.075	0.112	0.109	1.149	0.105		
Ti	0.034	0.020	0.008	0.018	0.064	0.016	Al <sup>VI</sup>	0.045
Sum	4.000	4.000	4.000	4.000	4.000	4.000	Ti	0.020
							Cr	0.004
Mg	0.120	0.338	0.253	0.404	0.008	0.072	Fe <sup>2+</sup>	0.217
Fe <sup>2+</sup>	2.854	3.618	3.683	3.823	0.884	2.842	Fe <sup>3+</sup>	0.040
Mn	1.120	0.449	0.165	0.095	4.023	1.873	Mg	0.823
Ca	1.905	1.614	1.905	1.644	1.049	1.124	Sum	2.000
Sum	5.999	6.019	6.006	5.966	5.965	5.911		

For garnet, cations based on 48 valencies including 10 cations in the tetrahedral and octahedral site to calculate Fe<sup>3+</sup>; for clinopyroxene, sum of cations is four. Numbers of stages are given in the text and Fig. 3d.

\*Calculated.

around 0.08 p.f.u (Table 5). Epidote composition varies strongly between 35 and 57 mol % pistacite component. Plagioclase is pure albite (An<sub>0.005-0.01</sub>) and titanite has about 20% of Ca(Al,Fe<sup>3+</sup>)SiO<sub>4</sub>(F,OH) component. Stilpnomelane is characterized by  $X_{Fe}$  of 0.73–0.75,  $X_K$  [K/(K + Na)] of 0.80–0.87 and an Mn content of 0.15–0.19 p.f.u.

#### *Metapelites and metapsammites of the Eastern belt*

Shales and sandstones with variable contents of phyllosilicates and quartz are the most common rock type in the Eastern belt. Whereas the shales are characterized by a penetrative cleavage, the sandstones, which may be mainly classified as litharenites, occasionally show a weak incipient banding with millimetre to centimetre spacing

into phyllosilicate-rich and quartz-rich domains. The metapsammitic rocks still exhibit relic clastic components to a large extent. Strongly angular to subrounded clasts of quartz are dominant. Albite clasts (sometimes with myrmekitic textures) are also abundant. Moreover, the frequent occurrence of partly perthitic K-feldspar clasts and of coarse white mica and chlorite as well as of rare biotite is a characteristic feature, whereas titanite, rutile, tourmaline, zircon, apatite and epidote are typical components of the heavy mineral spectrum. Among the lithic clasts are former mudstones (rip-up clasts), argillites, phyllites, siltstones, quartzites, cherts, mylonites and even scarce meta-ironstone and a fossiliferous limestone.

Indicative of very low grade metamorphism are oriented newly grown white mica and chlorite in phyllo-

Table 2: Representative analyses of epidote and pumpellyite

	Epidote					Pumpellyite				
	96CH113					96CH-71	Fo96-14	Fo96-15		
	I	IIa	IIb	IIc	III			I	II	
SiO <sub>2</sub>	37.55	37.36	37.52	37.31	37.60	36.17	36.73	SiO <sub>2</sub>	37.05	38.35
TiO <sub>2</sub>	0.12	0.10	0.10	0.12	0.04	0.05	0.11	TiO <sub>2</sub>	0.06	0.03
Al <sub>2</sub> O <sub>3</sub>	26.84	23.69	23.98	23.56	24.53	22.58	21.01	Al <sub>2</sub> O <sub>3</sub>	24.79	25.37
Fe <sub>2</sub> O <sub>3</sub>	7.62	12.68	12.65	13.25	11.02	13.52	16.23	Fe <sub>2</sub> O <sub>3</sub> *	2.99	0.15
MnO	0.10	0.23	0.12	0.22	0.16	0.89	0.28	FeO	3.33	6.29
MgO	0.02	0.00	0.00	0.01	0.00	0.00	0.02	MnO	0.13	0.20
CaO	23.46	22.95	23.15	22.86	23.39	23.76	23.08	MgO	2.22	0.52
H <sub>2</sub> O	3.75	3.73	3.74	3.73	3.75	3.67	3.69	CaO	22.61	22.43
Sum	99.46	100.74	101.26	101.06	100.49	100.64	101.15	Na <sub>2</sub> O	0.03	0.07
								H <sub>2</sub> O*	6.45	6.48
Si	3.000	3.000	3.000	3.000	3.000	3.000	3.000	Sum	99.66	99.89
Al	2.527	2.242	2.260	2.233	2.307	2.007	2.002			
Fe	0.458	0.766	0.761	0.802	0.662	0.988	0.991	Si	5.976	6.176
Mn	0.006	0.014	0.008	0.014	0.010	0.044	0.019	Al	4.712	4.817
Mg	0.003	0.000	0.000	0.001	0.000	0.000	0.002	Ti	0.007	0.004
Ti	0.007	0.006	0.006	0.007	0.003	0.003	0.007	Fe <sup>3+</sup>	0.363	0.018
Sum	3.001	3.028	3.035	3.057	2.982	3.042	3.021	Sum	5.082	4.839
Ca	2.008	1.974	1.983	1.969	1.999	1.998	2.006	Fe <sup>2+</sup>	0.449	0.847
								Mn	0.018	0.027
OH	2.000	2.000	2.000	2.000	2.000	2.000	2.000	Mg	0.533	0.125
								Sum	1.000	1.000
								Ca	3.908	3.871
								Na	0.008	0.022
								Sum	3.916	3.897
								OH	4.000	4.000

For epidote, cations based on Si = 3; H<sub>2</sub>O calculated on the basis of OH = 2. For pumpellyite, cations based on 49 negative valencies; H<sub>2</sub>O calculated on the basis of OH = 4; estimation of Fe<sup>2+</sup> by assuming half of X-position filled with divalent cations. Numbers of stages (roman numbers) are given in text and Fig. 3.

\*Calculated.

silicate layers of the incipient tectonic banding, but also recrystallized calcite and quartz starting to recrystallize in the matrix. Tectonic banding originates as the phyllosilicate-rich layers become relatively enriched by progressive removal of quartz and albite clasts between these phyllosilicates through pressure solution processes. Elongated quartz or albite grains with concave boundaries between oriented phyllosilicates are frequently observed in phyllosilicate-rich rocks.

Metamorphic phyllosilicates are distinctly smaller than the detrital ones. Detrital and metamorphic white micas

show significantly different compositions (see Fig. 5a, b, below) as typically found in sample 96CH-10 from Isla Meinhold (45°36.8'S, 74°06.7'W). Detrital white mica is muscovite with Si contents often between 3.1 and 3.2 p.f.u., Ti contents of 0.01–0.05 p.f.u., 4–10 mol % paragonite component and  $X_{Mg}$  of 0.40–0.65. However, all metamorphic white mica is phengite exhibiting a more restricted range of composition with 3.35–3.45 Si p.f.u., only 2 mol % paragonite component, and an  $X_{Mg}$  of 0.60–0.67.  $X_{Mg}$  in metamorphic chlorite also varies only between 0.48 and 0.57, and its Si contents are around 5.6 p.f.u.

Table 3: Representative analyses of amphibole

Amphibole										
	96CH113					Fo96-15	96CH-71	Fo96-14		
	I	II	IIIa	IIIb	IV	V		I	II	
SiO <sub>2</sub>	41.39	55.98	52.23	51.89	48.58	52.85	53.28	50.35	51.59	50.92
TiO <sub>2</sub>	0.33	0.02	0.07	0.03	0.13	0.05	0.01	0.10	0.10	0.10
Al <sub>2</sub> O <sub>3</sub>	13.85	0.93	3.30	3.64	6.73	1.32	0.89	4.47	3.55	3.86
Fe <sub>2</sub> O <sub>3</sub>	6.45	2.34	3.95	4.99	4.64	1.33	0.00	7.87	3.34	11.98
FeO	16.57	4.63	11.10	10.14	14.16	16.93	17.00	14.19	12.05	7.24
MnO	0.35	0.08	0.23	0.25	0.28	0.37	0.30	0.36	0.28	0.36
MgO	5.60	19.88	14.02	13.90	10.63	11.98	11.97	9.73	13.62	12.59
CaO	9.70	12.41	11.45	11.03	11.18	12.07	12.34	9.21	11.74	9.10
Na <sub>2</sub> O	2.62	0.37	0.87	0.96	1.25	0.38	0.27	1.82	0.78	1.40
K <sub>2</sub> O	0.75	0.03	0.07	0.10	0.20	0.10	0.10	0.32	0.11	0.18
F	0.00	0.00	0.06	0.00	0.08	0.17	0.10	0.00	0.04	0.12
Cl	0.00	0.00	0.00	0.01	0.00	0.01	0.00	0.00	0.01	0.00
H <sub>2</sub> O	1.97	2.13	2.04	2.06	1.99	1.94	1.95	2.04	2.03	2.01
Sum	99.63	98.83	99.40	99.04	99.82	99.49	98.23	100.65	99.25	99.87
Si	6.304	7.873	7.582	7.546	7.175	7.824	7.994	7.412	7.539	7.377
Al <sup>IV</sup>	1.696	0.127	0.418	0.454	0.825	0.176	0.006	0.588	0.461	0.623
Al <sup>VI</sup>	0.790	0.027	0.147	0.170	0.346	0.054	0.150	0.187	0.151	0.037
Ti	0.038	0.003	0.008	0.003	0.015	0.006	0.001	0.012	0.010	0.011
Fe <sup>3+</sup>	0.739	0.248	0.432	0.546	0.516	0.148	0.000	0.872	0.367	1.307
Fe <sup>2+</sup>	2.110	0.545	1.347	1.233	1.748	2.096	2.133	1.746	1.473	0.878
Mn	0.045	0.009	0.028	0.031	0.035	0.046	0.038	0.045	0.034	0.044
Mg	1.271	4.167	3.034	3.013	2.340	2.643	2.677	2.135	2.965	2.718
Sum	5.000	5.000	5.000	5.000	5.000	5.000	5.000	5.000	5.000	5.000
Ca	1.583	1.870	1.781	1.718	1.769	1.914	1.984	1.453	1.838	1.413
Na	0.774	0.100	0.244	0.272	0.358	0.110	0.078	0.519	0.220	0.393
K	0.145	0.006	0.013	0.019	0.038	0.018	0.019	0.061	0.021	0.033
Sum	2.502	1.976	2.038	2.009	2.165	2.04	2.084	2.033	2.082	1.839
Cl	0.000	0.000	0.000	0.002	0.000	0.002	0.000	0.000	0.002	0.000
F	0.000	0.000	0.028	0.000	0.037	0.079	0.045	0.000	0.019	0.055
OH	2.000	2.000	1.972	1.998	1.963	1.919	1.954	2.000	1.979	1.944

Cations based on 46 valencies and sum of cations = 13 except for Ca, Na and K for estimation of Fe<sup>3+</sup>; H<sub>2</sub>O calculated; sum corrected for F and Cl. Numbers of generations (roman numbers) are given in text and Fig. 3.

#### *Meta-ironstones and metacherts of the Eastern belt*

Rare rock types are lensoid intercalations of white metachert beds up to several tens of metres thick often associated with intercalations of Fe- and Mn-rich layers of centimetre to 1 m thickness. According to geochemical analyses by Godoy *et al.* (1984), these metalliferous intercalations are comparable with pelagic oceanic sediments. The metachert intercalations are mainly tectonic lenses within dark slates, which are internally deformed by recumbent chevron folds.

A meta-ironstone intercalated with metacherts, sample 96CH-85 from a small island at the northern end of Isla Chalacayec (44°56.9'S, 73°45.4'W), is a dark finely banded micritic carbonate rock consisting of a very fine-grained matrix of siderite, chlorite and graphite containing fine-grained oriented, ovoid chlorite aggregates. Siderite and chlorite may form monomineralic bands of millimetre thickness. The rock is broken into clasts healed and cut by veins of various generations filled with quartz, chlorite and/or calcite. Chlorite is

Table 4: Representative analyses of stilpnomelane, biotite and white mica

	Stilpnomelane			Biotite		White mica				
	Fo96-15	96CH-71	96CH-72	96CH-71	Fo96-14	96CH113		Fo96-15	96CH-10	96CH-37
						I	II			
SiO <sub>2</sub>	51.06	46.52	45.55	37.65	37.03	52.05	46.48	51.18	51.26	50.50
TiO <sub>2</sub>	0.03	0.03	0.00	1.17	1.31	0.18	0.38	0.04	0.02	0.12
Al <sub>2</sub> O <sub>3</sub>	5.66	6.07	6.07	14.10	15.45	22.85	28.09	24.34	26.87	27.19
FeO	24.95	25.43	29.85	22.36	19.73	3.15	4.10	5.41	2.95	3.52
MnO	1.09	1.26	1.64	0.21	0.15	0.01	0.00	0.13	0.06	0.09
MgO	5.24	7.42	4.18	9.98	11.30	4.44	2.58	2.42	2.62	2.39
BaO	0.04	0.68	0.02	0.26	0.08	0.44	2.68	0.07	0.14	0.46
Na <sub>2</sub> O	0.43	0.41	0.25	0.04	0.05	0.12	0.47	0.02	0.14	0.22
K <sub>2</sub> O	2.93	2.05	1.76	9.21	9.50	10.79	9.67	11.61	10.44	10.59
F				0.36	0.30	0.00	0.03	0.00	0.07	0.11
H <sub>2</sub> O	5.38	5.22	5.11	3.70	3.75	4.40	4.31	4.39	4.44	4.40
Sum	96.81	95.16	94.51	98.99	98.59	98.52	98.88	99.68	99.00	99.56
Si	8.532	8.012	8.011	5.840	5.697	7.092	6.453	6.991	6.878	6.805
Al <sup>IV</sup>	0.468	0.988	0.989	2.160	2.303	0.908	1.548	1.009	1.122	1.195
Al <sup>VI</sup>	0.647	0.244	0.270	0.417	0.498	2.761	3.048	2.909	3.127	3.124
Ti	0.004	0.004	0.000	0.137	0.152	0.018	0.039	0.004	0.002	0.012
Fe <sup>2+</sup>	3.485	3.598	4.298	2.900	2.538	0.359	0.406	0.618	0.331	0.397
Fe <sup>3+</sup>	0.000	0.065	0.092	0.000	0.000	0.000	0.073	0.000	0.000	0.000
Mn	0.154	0.184	0.244	0.028	0.020	0.001	0.000	0.015	0.006	0.011
Mg	1.304	1.905	1.096	2.307	2.592	0.902	0.534	0.493	0.524	0.480
Sum	5.594	6.000	6.000	5.789	5.800	4.051	4.100	4.044	3.990	4.023
Ba	0.003	0.046	0.000	0.016	0.005	0.023	0.146	0.004	0.008	0.024
Na	0.139	0.137	0.173	0.011	0.016	0.033	0.127	0.006	0.036	0.058
K	0.624	0.450	0.530	1.822	1.865	1.875	1.712	2.023	1.787	1.820
Sum	0.766	0.634	0.704	1.861	1.886	1.931	1.985	2.035	1.830	1.905
F				0.177	0.147	0.000	0.012	0.000	0.029	0.048
OH	6.000	6.000	6.000	3.823	3.853	4.000	3.988	4.000	3.971	3.952

For stilpnomelane, cations based on 47.375 valencies neglecting K + Na; Fe<sup>3+</sup> estimated assuming 15 cations; OH = 6. For biotite, cations based on 44 valencies; OH + F = 4; sum corrected for F; H<sub>2</sub>O calculated. For white mica, cations based on 44 valencies; OH + F = 4; sum of octahedral cations = 4.1 for estimation of Fe<sup>3+</sup>; H<sub>2</sub>O calculated; sum corrected for F. Numbers of generation (roman numbers) are given in text.

characterized by variable Si content (5.2–5.7 p.f.u.), very low  $X_{Mg}$  (0.21–0.3) and a notable Mn content (0.14–0.2 p.f.u.). Siderite contains 9 mol % rhodochrosite, 13–15 mol % magnesite and 3 mol % calcite component, whereas calcite contains 12–18 mol % rhodochrosite, 2 mol % siderite and 1 mol % magnesite component.

Metacherts are found associated with these meta-ironstones in Isla Chalacayec. These may contain some white mica, and are recrystallized to microquartz (5–10 µm) with relics of strongly deformed radiolarians forming lensoid 'ghosts' of microquartz aggregates (100 µm diameter) among the white micas. The amount of radiolarian

relics varies. The degree of recrystallization inhibits determination (H.J. Gursky, personal communication, 1997). Other rocks lack relics and may be termed microquartzites.

### The Western belt

In contrast to the rocks of the Eastern belt, in the compositionally similar metapsammopelitic schists of the Western belt any primary sedimentary structures are completely obliterated and a flat-lying to gently NE-dipping penetrative crenulation foliation  $S_2$  developed

Table 5: Representative analyses of chlorite

Chlorite							
	96CH113			Fo96-15	96CH-10	96CH-71	Fo96-14
	la	lb	II				
SiO <sub>2</sub>	24.91	25.50	25.44	25.65	26.63	27.55	26.21
TiO <sub>2</sub>	0.02	0.11	0.11	0.05	0.00	0.02	0.05
Al <sub>2</sub> O <sub>3</sub>	18.43	17.84	19.68	18.92	19.58	17.04	19.73
FeO	34.17	33.52	30.31	30.13	22.03	27.64	24.74
MnO	0.73	0.52	0.45	0.36	1.72	0.34	0.29
MgO	9.41	9.54	12.18	11.55	16.53	14.13	16.50
CaO	0.17	0.26	0.01	0.10	0.02	0.07	0.07
Na <sub>2</sub> O	0.04	0.19	0.00	0.01	0.09	0.01	0.01
K <sub>2</sub> O	0.01	0.04	0.03	0.04	0.10	0.05	0.00
H <sub>2</sub> O	10.78	10.74	11.10	10.91	11.32	11.11	11.32
F	0.00	0.07	0.03	0.06	0.08	0.02	0.15
Sum	98.75	98.32	99.35	97.80	98.21	98.00	98.99
Si	5.539	5.673	5.490	5.623	5.632	5.943	5.520
Al <sup>IV</sup>	2.461	2.327	2.510	2.377	2.377	2.057	2.480
Al <sup>VI</sup>	2.368	2.351	2.495	2.514	2.496	2.275	2.417
Ti	0.003	0.019	0.018	0.008	0.000	0.002	0.007
Fe	6.354	6.236	5.470	5.525	3.890	4.986	4.358
Mn	0.137	0.098	0.083	0.067	0.308	0.061	0.052
Mg	3.119	3.164	3.917	3.776	5.202	4.543	5.179
Ca	0.040	0.061	0.003	0.025	0.003	0.015	0.015
Na	0.019	0.082	0.000	0.006	0.039	0.004	0.003
K	0.003	0.012	0.007	0.011	0.026	0.013	0.000
Sum	12.043	12.021	11.993	11.932	11.964	11.900	12.030
F	0.000	0.046	0.018	0.042	0.000	0.014	0.101
OH	16.000	15.936	15.982	15.958	16.000	15.986	15.899

Cations based on 56 valencies and OH + F = 16; sum corrected for F; H<sub>2</sub>O calculated. Numbers of generations (roman numbers) are given in text and Fig. 3.

subparallel to bedding and relic  $S_1$  as a transposition foliation. The generation of a NW–SE to NNW–SSE-trending stretching lineation parallel to axes of minor isoclinal rootless  $F_2$  folds is prominent.

A further prominent feature of the Western belt distinguishing it from the Eastern belt is the abundance of greenschist intercalations. These are lensoid bodies of several hundred metres length within the mainly metapsammopelitic rocks. According to Godoy *et al.* (1984), their chemical composition is close to that of MORBs. Some metacherts and Fe–Mn-rich rock types are associated with the greenschists.

#### *Foliated metabasites of the Western belt*

This rock type is the most common metabasite within the Western belt. Samples 96CH-110 and Fo96-35 from

the western coast of Isla Gertrudis (44°34.6'S, 73°53.6'W) are typical examples. The schistosity shows tight folds of different size, also affecting quartz bands parallel to the foliation. Some thick quartz veins that also contain pyrite cut through the folds. Kink bands of centimetre scale are conspicuous.

The mineral assemblage is amphibole–epidote–quartz–albite–titanite–ilmenite containing accessory apatite. Dominating amphibole is present as strongly oriented, idioblastic prisms up to 1 mm long, which are synkinematic to the main foliation  $S_2$ . Amphibole shows pronounced optical zoning with pale cores similar to epidote, which is also oriented parallel to  $S_2$ . Lenticular domains of polygonal quartz and elongated quartz and albite crystals are controlled by the main crystal faces of amphibole. Within quartz and albite a relic internal  $S_1$

is defined by small oriented, rounded epidote inclusions, and is oblique with respect to the principal external foliation  $S_2$ . Albite porphyroblasts overgrew  $S_2$  crenulation hinges, being a late postkinematic phase.

Amphibole (see Fig. 4b, below) is magnesio-hornblende with tschermakitic hornblende at the rims. From cores to rims there is a continuous decrease in  $X_{Mg}$  from 0.65 to 0.50 with decreasing Si content from 7.3 to 6.3 p.f.u. The  $Na^{M4}$  content is up to 0.2 p.f.u.;  $(Na + K)^A$  is as high as 0.4 p.f.u. Epidote contains 44–61 mol % pistacite component; the higher values were determined at the mineral rims. Titanite has 6–16 mol %  $Ca(Al, Fe^{3+})SiO_4(F, OH)$  component.

Sample Fo96-14 is from the western coast of Isla Venezia (45°20'2'S, 74°19'W), where the metabasites form a conspicuous morphological ridge inside the surrounding metapelites. The metabasites show two different textural and compositional zones, which form alternating bands of millimetre thickness. Domain I is coarser grained with the constituent minerals less oriented than in domain II. It is composed of epidote and chlorite, with minor amphibole, biotite and albite. These constituents may even form nearly monomineralic domains of millimetre scale. Domain II is very fine grained with dominant well-oriented amphibole and minor chlorite, titanite and quartz. Recrystallized amphiboles can be observed in rare  $S_2$  crenulation hinges. Large albite porphyroblasts with sigmoidal inclusion trails in the cores and inclusion-free rims grew across the foliation. Inclusions are mainly epidote as well as minor amphibole and titanite. Similarly, biotite grew unoriented as a late static phase across oriented amphibole and chlorite. However, biotite is sometimes enclosed within albite porphyroblasts, which are therefore interpreted as the latest grown minerals.

Amphibole is actinolite or actinolitic hornblende with  $X_{Mg}$  around 0.7–0.8 and  $Na^{M4}$  content around 0.2–0.3 p.f.u. Biotite has an intermediate  $X_{Mg}$  around 0.50, similar to chlorite (0.53–0.56). Epidote composition varies considerably from 67 to 100% pistacite component.

#### *Garnet-bearing metabasite of the Western belt*

A massive weakly foliated garnet-bearing metabasite (samples 96CH-113 and Fo96-39) with a faint pillow structure, crossed by veinlets and pods of quartz, occurs on a small island adjacent to the SE end of Isla Carmencita (44°32'76'S, 73°54'29'W). It is a unique rock type among the greenschists as a result of occurrence of garnet, but a key rock for understanding the  $P$ – $T$  evolution.

Garnet (Fig. 2) shows inclusions of quartz, epidote and titanite in equal proportion, as well as of rare amphibole and chlorite, all oriented along trails that are straight in the core of garnet grains and sigmoidal toward the edges. This internal  $S$  is oblique with respect to the external

principal foliation  $S_2$  defined mainly by oriented amphiboles and deflected around the garnet grains. Orientation of the sigmoidal internal  $S_1$  is similar over the thin-sections of this rock type, suggesting late garnet growth synkinematically with the formation of  $S_2$ , which obviously originated as a crenulation cleavage. Garnet is partially pseudomorphosed by undeformed chlorite to variable extent. Finally, the chloritized garnets are surrounded by later grown albite, which also forms small earlier grown blasts with tiny epidote inclusions defining a rotated foliation.

Amphiboles are present in two populations of different size: the larger ones are zoned with a nearly colourless core. They are partly altered to chlorite. Epidote is abundant and has more strongly coloured rims. Titanite forms chains of minute crystals. White mica is present in large laths that may be slightly oriented similar to chlorite and amphibole. Magnetite occurs as minor phase.

Mn distribution in garnet is typically bell shaped with up to 18 mol % spessartine in the core decreasing to 3 mol % at the rim. However, element distribution maps of Ca and Mg clearly show a marked oscillatory zoning (Fig. 3). Thus, on this basis, roughly four major compositional zones may be distinguished that also contain inclusions of epidote, chlorite and amphibole with notably variable composition. From core to rim the grossular content decreases from 36 to 27 mol %, whereas the pyrope content increases from 2.4 to 6.4 mol % and the almandine content from 46 to 66 mol % (Table 1).

Amphiboles are all Ca amphiboles with rather variable compositions and irregular zoning. Five generations may be differentiated (Table 3 and Fig. 4a), as follows. Two inclusions of ferroan pargasitic hornblende within garnet may represent magmatic relics (amphibole I). Larger matrix amphiboles have nearly colourless cores representing actinolites with high  $X_{Mg}$  exceeding 0.8 (amphibole II) that are sharply overgrown by a bluish green actinolitic to magnesio-hornblende with an  $X_{Mg}$  of 0.55–0.70 and an elevated  $Na^{M4}$  content of 0.20–0.55 p.f.u. (amphibole IV). Smaller crystals have compositions similar to the rims of the larger crystals. Zoning is rather irregular, but shows a tendency to increasing Ca and decreasing Na and Fe towards the rims. Outermost rims are actinolites again, but with  $X_{Mg}$  of 0.55–0.60 (amphibole V). Inclusions in garnet (amphibole III) are similar to amphibole IV. However, those inclusions in the cores of garnets are still actinolites with high  $X_{Mg}$  of around 0.7 and low  $Na^{M4}$  content of around 0.2 p.f.u. changing to  $X_{Mg}$  of around 0.55 and  $Na^{M4}$  content of around 0.35 p.f.u. for the magnesio-hornblendes within the rim zone of garnet. Similar decrease of  $X_{Mg}$  and increase in  $Na^{M4}$  with decreasing Si contents is also observed for amphibole IV of the matrix. Epidotes show strong zoning with a relatively homogeneous core with about 45 mol % of pistacite component (epidote I) that

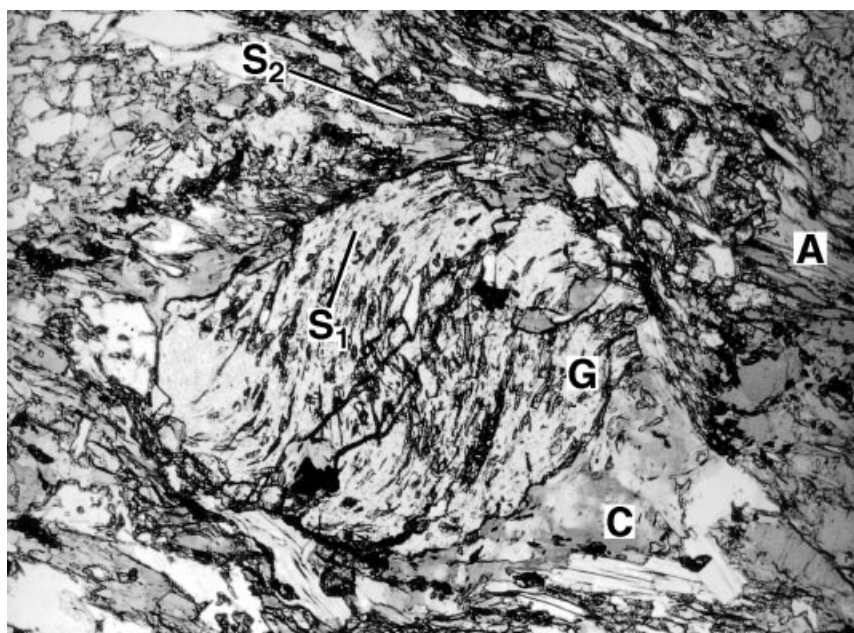


**Fig. 2.** Garnet porphyroblast synkinematic with respect to  $S_2$  in metabasite sample 96CH-113. Position of  $S_1$  and  $S_2$  is marked. A, amphibole; C, chlorite; G, garnet. Plane-polarized light. Width of photograph represents 1.2 mm.

is unconformably overgrown by a rim with increased pistacite contents up to 50–78 mol % that are also found in smaller grains (epidote III; Table 2). Epidote inclusions in garnet have generally more than 75 mol % pistacite component (epidote II). The composition of chlorite in the matrix (chlorite II) that replaces garnet and amphibole is fairly uniform, with Si contents of 5.4–5.5 p.f.u., somewhat elevated Mn contents of up to 0.09 p.f.u. and  $X_{Fe}$  slightly decreasing from core to rim (from 0.59 to 0.56). However, chlorite inclusions in garnet (chlorite I) differ considerably by their higher  $X_{Fe}$  of 0.67, Si of 5.54–5.67 p.f.u. and Mn contents up to 0.14 p.f.u. (Table 5). Furthermore, chlorite I is comparable with inclusions of other minerals in garnet because of its oval shape and size. By contrast, chlorite II has irregular contacts with replaced garnet and a considerably larger grain size. White micas show a considerable compositional range of Si contents from 3.22 to 3.56 p.f.u. (Fig. 5). In a larger crystal, a zonation is indicated with Si content of 3.37 p.f.u. in the core (white mica I) and 3.27 p.f.u. in the rim (white mica II). The latter value is similar to those in smaller crystals in the matrix.  $X_{Mg}$  increases systematically from 0.5 to 0.75 with increasing Si content. Titanite contains about 3–7 mol %  $Ca(Al,Fe^{3+})SiO_4(F,OH)$  component. Albite is almost pure ( $An_{01}$ ).

The systematic compositional variation of the zoned minerals and different generations of inclusion minerals strongly suggests successive preservation of continuous reactions within compositional domains representing local equilibrium stages. The correlation of the different

mineral compositions with four stages of equilibration is given in Table 6, and representative analyses in Tables 1–5. The second stage is defined by the growth of garnet synkinematically with  $D_2$ . One stage before garnet growth and two stages after garnet growth are thus recognized. The growth of garnet may be further subdivided into four successive steps of equilibration defined by the composition of the garnet zones best represented by the Ca zonation (Fig. 3) and their respective included minerals.

#### *Metapelites and metapsammites of the Western belt*

In the Western belt the metapsammopelitic rocks are foliated with pronounced alternating bands rich in micas or quartz generally represented by a crenulation cleavage  $S_2$ , which defines microlithons up to 2 cm wide. The rocks show abundant quartz segregations of different generations. The metamorphic mineral assemblage is fairly uniform: quartz–albite–white mica–chlorite–titanite–graphite. The phyllosilicates are well oriented in the  $S_1$  and  $S_2$  foliation.  $S_2$  crenulation hinges show recrystallization of white micas. Epidote, calcite, tourmaline, and magnetite or ilmenite are common accessories. Conspicuous idiomorphic millimetre-sized albite porphyroblasts are a characteristic feature of this belt and are mainly bound to layers rich in white mica. They have grown after the development of the main foliation  $S_2$  with graphite inclusion trails well marking the outline of the former  $S_2$  crenulation foliation. Sometimes the albite porphyroblasts have a rim free of in-

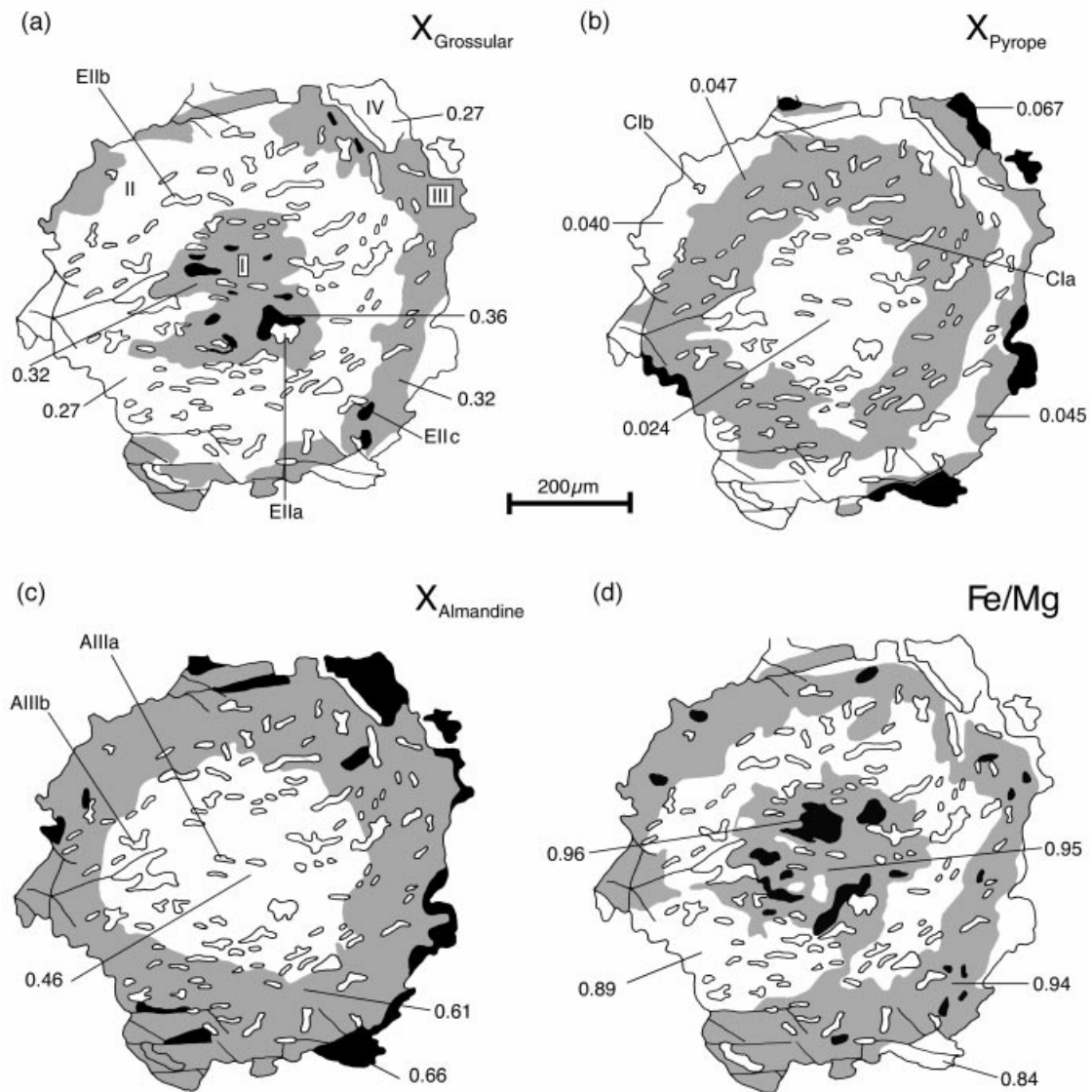


**Fig. 3.** Characteristic element distribution maps of garnet in sample 96CH-113. Locations of inclusions (A, amphibole; C, chlorite; E, epidote) are given with indices as in Tables 1–5. Redrawn element distribution of relative X-ray intensities is based on 41 538 points and increases in the order white–grey–black. The characteristic oscillation zoning should be noted. For each zone a quantitative representative analysis is given as a ratio at the point analysed or complete in Tables 1–5. The rims of the garnet are not complete, as a result of decomposition to retrograde chlorite.

clusions. Within the polygonal quartz matrix, albite exhibits the same size and outline as quartz. The development of the main foliation as quartz- and phyllosilicate-rich bands suggests that pressure solution was a predominant mechanism of deformation.

Five samples of psammopelitic schists all from close to the contact with the Eastern belt were analysed: 96CH-32 (SE coast of Isla Venezia: 45°21.7'S, 74°14.5'W); Fo96-25 (small island near the SE end of Isla Kent: 45°10'S, 74°14.7'W); 96CH-37 (NW of Isla Venezia:

45°20.2'S, 74°02'W); 96CH-35 (SW edge of Isla Dring: 45°02'S, 74°02'W); 96CH-103 (SE edge of Isla Jesus: 44°44.5'S, 73°49'W).

White micas are generally phengites with a similar compositions in most samples (Fig. 5a, b) ranging from 3.15 p.f.u. (mostly at the rims) to 3.35 p.f.u. Only sample 96CH-37 contains phengites with Si contents ranging between 3.3 and 3.4 p.f.u. In sample 96CH-103 maximum Si contents reach only 3.2 p.f.u. In this rock, grain size of recrystallized white mica and quartz

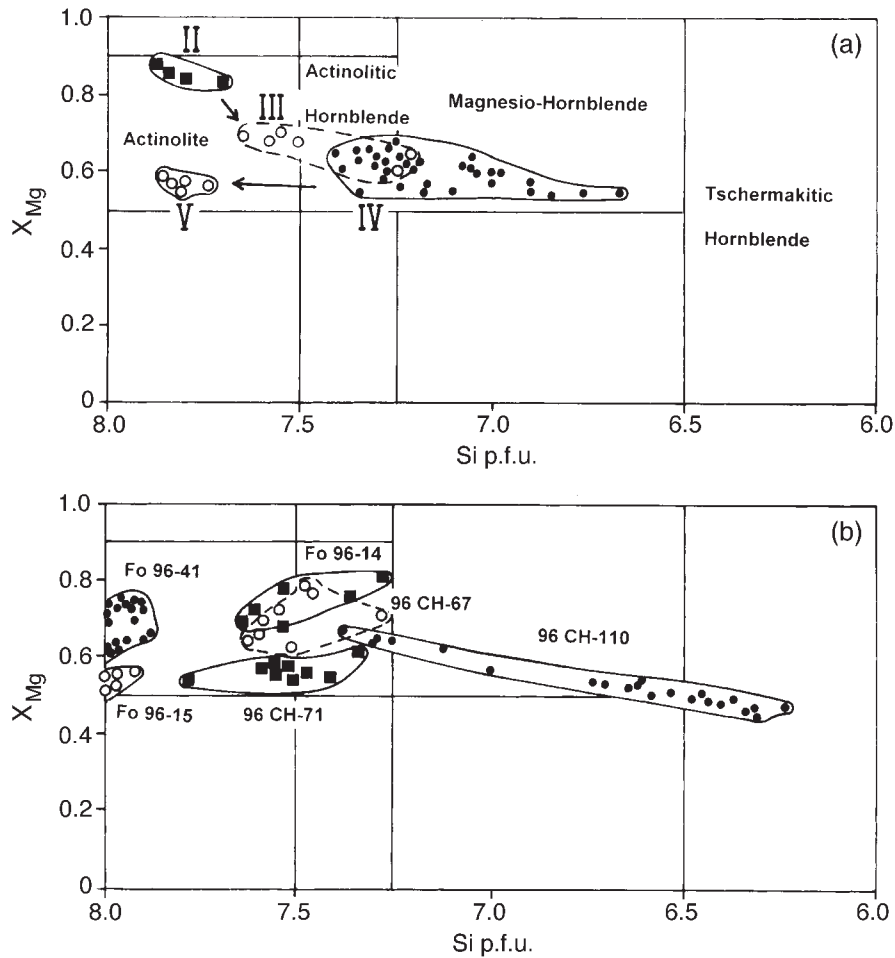


Fig. 4.  $X_{Mg}$ -Si variation of amphiboles of (a) different generations (II, III, IV and V) in garnet-bearing metabasite (samples 96CH-113, Fo96-39) and (b) of various greenschists and meta-ironstones. Nomenclature after Leake (1978).

is smaller than in other samples. Compositions of the white micas in all five samples are close to the ideal Tschermak substitution line, indicating the lack of any ferri-muscovite component. The paragonite component is lower than 5 mol %, Ti contents are around 0.01 p.f.u. and  $X_{Mg}$  between 0.45 and 0.6 without notable regular variation with Si contents. Titanite contains about 7 mol % of  $Ca(Al,Fe^{3+})SiO_4(F,OH)$  component. Relatively uniform and low are Si contents (5.15–5.4 p.f.u.) and  $X_{Mg}$  (0.34–0.4) of chlorite. Plagioclase is almost pure albite.

#### *Meta-ironstones of the Western belt*

Meta-ironstones in the Western belt are characterized by an Fe-rich, bulk-rock chemistry resulting in growth of abundant stilpnomelane during metamorphism. They are mostly associated with greenschists. They generally exhibit a characteristic banding, often on a millimetre

scale. The thickness of their intercalations is up to several tens of centimetres.

Some meta-ironstones can also be called stilpnomelane quartzites, for example, those occurring near the western end of Isla Jesus (Fo96-41b, Fo96-41d: 44°44'6"S, 73°54'1"W). In these well-banded siliceous rocks, laminae with very fine-grained titanite and graphite alternate with equigranular polygonal quartz-rich bands containing abundant rosettes of mainly unoriented stilpnomelane and some isolated chlorite, amphibole, calcite and white mica. Preferred orientation of these minerals is weak. Some pyrite may be present as well.

White mica in sample Fo96-41d is phengite with Si contents ranging from 3.2 to 3.3 p.f.u. Amphibole is actinolite with low Na contents around 0.04 p.f.u. and  $X_{Mg}$  varying between 0.6 and 0.75. Chlorite compositions show Si between 5.56 and 5.66,  $X_{Mg}$  around 0.55 and Mn around p.f.u. in Fo96-41b, and Si between 5.2 and 5.45 p.f.u.,  $X_{Mg}$  around 0.35 and Mn around 0.12 p.f.u.

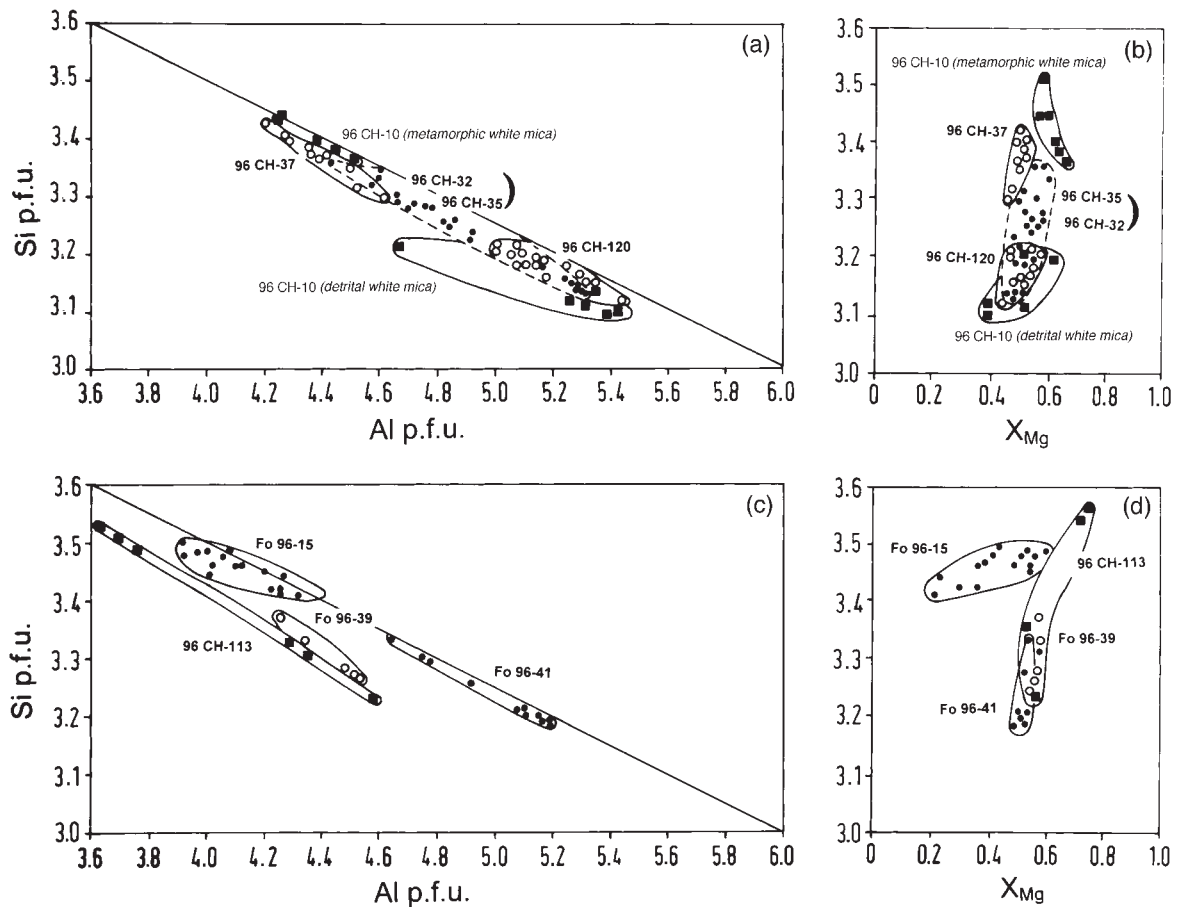


Fig. 5. Si–Al variation of white micas in (a) metapsammopelites and (c) metabasites;  $X_{Mg}/Si$  variation of white micas in (b) metapsammopelites and (d) metabasites.

in Fo96-41d. The  $Ca(Al,Fe^{3+})SiO_4(F,OH)$  component in titanite varies from 8 to 20 mol %. Plagioclase is almost pure albite. Stilpnomelane is characterized by an  $X_{Fe}$  of 0.68–0.71 in sample Fo96-41d and 0.59 in Fo96-41b, an  $X_K$  of 0.71–0.88 and an Mn content of 0.18–0.21 p.f.u.

Other meta-ironstones are laminated stilpnomelane-rich rocks (96CH-67, 96CH-71) occurring on a small island near the northern coast of Isla Dring ( $45^{\circ}11'7''S$ ,  $74^{\circ}16'8''W$ ), where lithological contacts between metapelites and greenschists are exposed. Within the greenschist bands, pods and lenses of stilpnomelane-bearing rocks are observed that are strongly banded. Bands of up to centimetre thickness may represent an original sedimentary lamination. Mineral assemblages within these laminae are: epidote–biotite–amphibole–quartz, epidote–stilpnomelane–quartz, amphibole–stilpnomelane–quartz–biotite or biotite–epidote–quartz–calcite. Also, domains of pure stilpnomelane with some calcite or epidote, or domains with nearly monomineralic epidote, occur. Some chlorite and titanite or

magnetite may also be present. Amphiboles and chlorite are well oriented, whereas biotite mostly grew obliquely to  $S_1$  and  $S_2$ . In some cases, the overgrowth of biotite around chlorite is apparent.

Amphibole (Fig. 4b) is actinolite or actinolic hornblende with  $Fe^{3+}$  contents of 0.6–0.8 p.f.u. and  $Na^{M4}$  around 0.4 p.f.u. Higher Si contents occur at the rims, corresponding to slightly higher  $X_{Mg}$ . Epidote generally has pistacite components of 80–100 mol %. Biotite is characterized by an intermediate  $X_{Mg}$  of 0.44–0.49, Ti of 0.05–0.08 p.f.u., Mn around 0.02 p.f.u. and 0.3 wt % F. Chlorite generally has a Si content around 6 p.f.u. and an  $X_{Mg}$  around 0.48. Stilpnomelane is characterized by an  $X_{Fe}$  of 0.63–0.65, an  $X_K$  of 0.71–0.80 and an Mn content of 0.13–0.19 p.f.u.

Sample 96CH-72 from the same locality contains additional bands composed of stilpnomelane and garnet. Garnets are mainly spessartine–almandine solid solutions with decreasing spessartine and andradite components from core to rim, whereas grossular and almandine components increase (Fig. 6). Pyrope contents are only

Table 6: Assemblages of mineral generations (roman numbers) assigned to successive equilibration stages calculated for the garnet-bearing metabasites 96CH-113 and Fo96-39

Stage	Reference						
	1	2a	2b	2c	2d	3	4
Garnet		I	II	III	IV		
Amphibole	II	IIIa	IIIb	IIIb	IIIb	IV	V
Epidote	I	IIa	IIb	IIc	IIc	III	III
Chlorite		Ia	Ia	Ib	Ib	II	II
White mica				I	I	II	II
T1 (°C)*		339	388	380	407		
T2 (°C)**					551		
T3 (°C)*		375	447	485	502		
P1 (kbar)*		7.5	8.5	9.9	9.4		
T4 (°C)*		332	404	436	454		
P2 (kbar)		6.4	7.5	8.7	8.2		
T5*					485		
P3					10.5		
T6						400	
P4						5.0	

Respective compositions of the mineral generations are shown in Table 1. The position of mineral inclusions is shown in Fig. 4. Quartz and albite were stable during all stages. Explanation of calculated temperatures T1–T6 and pressures P1–P4 is given in text.

\*Fe/Mg Garnet/Amphibole.

†Fe/Mg Garnet/Phengite.

References: 1, Graham & Powell (1984); 2, Massonne & Szpurka (1997); 3, Massonne (1995a); 4, Berman (1990) and Massonne (1995b).

1 and 2 mol %. The decreasing Fe<sup>3+</sup> suggests a dramatic change to more reducing conditions during prograde garnet growth. Stilpnomelane is characterized by an  $X_{\text{Fe}}$  of 0.78–0.81, an  $X_{\text{K}}$  of 0.75–0.95 and an Mn content of 0.19–0.26 p.f.u.

Sample 96CH-57 from the same locality is a stilpnomelane quartzite, with a polygonal matrix of quartz, some carbonate and randomly oriented stilpnomelane. Stilpnomelane is characterized by an  $X_{\text{Fe}}$  of 0.61–0.63, an  $X_{\text{K}}$  of 0.71–0.84 and an Mn content of 0.16–0.17 p.f.u.

## METAMORPHIC CONDITIONS

*P-T* conditions to decipher the metamorphic evolution of the rocks described above were estimated by three methods:

(1) we considered the *P-T* ranges of critical metamorphic assemblages known as metamorphic facies and information on the minimum *P-T* conditions for recrystallization of particular minerals, e.g. quartz, carbonate, white mica;

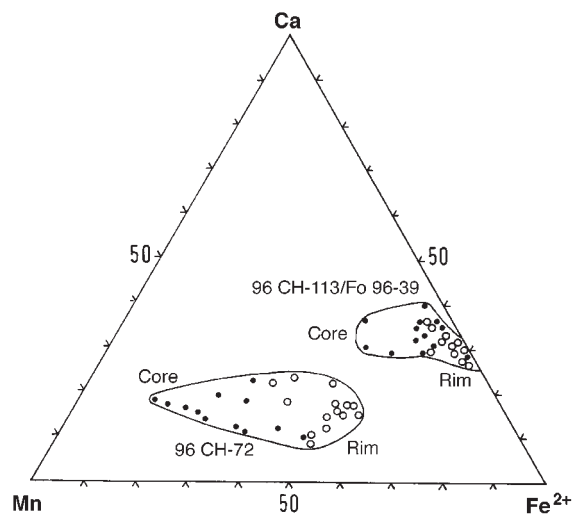


Fig. 6. Variation of garnet compositions.

(2) we used empirically and experimentally determined geothermometers such as the garnet–amphibole thermometer of Graham & Powell (1984);

(3) we conducted thermodynamic calculations of numerous mineral equilibria relevant to the assemblages observed here.

Because our resulting  $P$ - $T$  estimates depend strongly on the third method, further details are given below. Basically we applied the Ge0-Calc software package of Brown *et al.* (1989) with the data set of Berman (1988). In addition, we used the following thermodynamic data, compatible to Berman's data set, and including corresponding activity models:

(1) for pumpellyite: Mg-pumpellyite of Evans (1990);

(2) for chlorite: chlinochlore of Massonne (1995a);

(3) for amphibole: tremolite and glaucophane of Massonne (1995a);

(4) for white mica: muscovite, Mg-Al-celadonite and Fe-Al-celadonite of Massonne (1995b) with improvements given by Massonne & Szpurka (1997);

(5) for garnet: grossular, pyrope and almandine of Berman (1990) with additions made by Massonne (1995b).

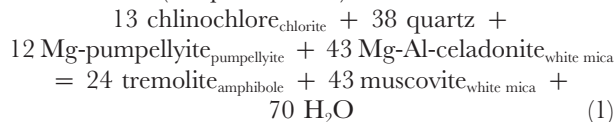
For clinozoisite we considered the activity model  $a_{\text{clinozoisite}} = 1 - X_{\text{pistacite}}$ .

## The Eastern belt

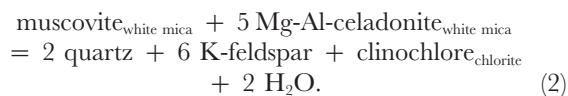
Existing temperature estimates for the peak metamorphic conditions of rocks of the Eastern belt are based on measurements of the illite crystallinity by Garrido (1987) and Hormazábal (1991) showing values corresponding to an upper anchimetamorphic stage with a slight tendency of increasing metamorphic grade from east to west. This is confirmed by the fabric of matrix quartz in metapsammites showing initial recrystallization. The degree of recrystallization allowing recognition of relics of radiolarians in metacherts from Isla Chalacayec also indicates very low grade conditions (H.-J. Gursky, personal communication, 1997). Furthermore, the metabasites of Isla Dring show typical assemblages of the pumpellyite-actinolite facies.

In addition, the  $P$ - $T$  position of the two multivariant mineral equilibria was thermodynamically determined:

in metabasite (sample Fo96-15):



in metapsammite (sample 96CH-10):



Although in the metabasite sample Fo96-15 actinolite

and chlorite show astonishingly homogeneous compositions, the strongly different pumpellyite compositions in matrix and veinlets are rather indicative of a non-equilibrium system. Being aware of this shortcoming, we concentrated on the coarse-grained veinlet assemblage, regarding this as an equilibrium domain developed near peak  $P$ - $T$  conditions. From the fabric and compositions of minerals described above, opening and filling of the white mica veins occurred during peak metamorphic  $P$ - $T$  conditions in the matrix, that is, the phengite zonation represents prograde increase of pressure and temperature near the pressure maximum.

In the metapsammite sample 96CH-10 the phyllosilicate-rich domains of the incipient tectonic banding may be regarded as equilibrium domains showing a relatively restricted compositional range of metamorphic white micas and chlorite. Although abundant potassic feldspar in these domains is of relic clastic origin, we assume that it took part in the reaction.

In Fig. 7, bands represent the  $P$ - $T$  range of both equilibrium reactions calculated from core and rim compositions covering the entire compositional range of corresponding solid solutions in the equilibrium domains of both samples that varied during the growth of the respective minerals. Considering that a similar maximum  $P$ - $T$  range was reached in both samples, this range is approximated by the intersectional area of both  $P$ - $T$  bands at 4.5–6 kbar and 250–280°C. However, both equilibria are dependent on water activity. This factor is assumed to be near unity, because calcite is lacking in the rocks studied.

## The Western belt

### Metabasites

Metabasites in the Western belt are characterized by assemblages transitional between greenschist and albite-epidote-amphibolite facies as defined by Evans (1990); typical assemblages for the albite-epidote-amphibolite facies appear in samples 96CH-110 and Fo96-35. They are characterized by the presence of albite with actinolitic hornblende and the absence of chlorite. Samples 96CH-113 and Fo96-39 contain garnet together with actinolitic hornblende and epidote. On the other hand, the presence of primary chlorite with actinolitic hornblende in sample Fo96-14 and the presence of pure actinolite and chlorite in meta-ironstone Fo96-41 indicate greenschist facies conditions. According to Evans (1990), the transition between the two facies, marked by the first appearance of spessartine-poor garnet in metabasites, is around 500°C. On the other hand, the peak temperature range for the metabasites of the Western belt is estimated to be roughly 350–400°C according to the plagioclase-amphibole thermometer of Spear (1980).

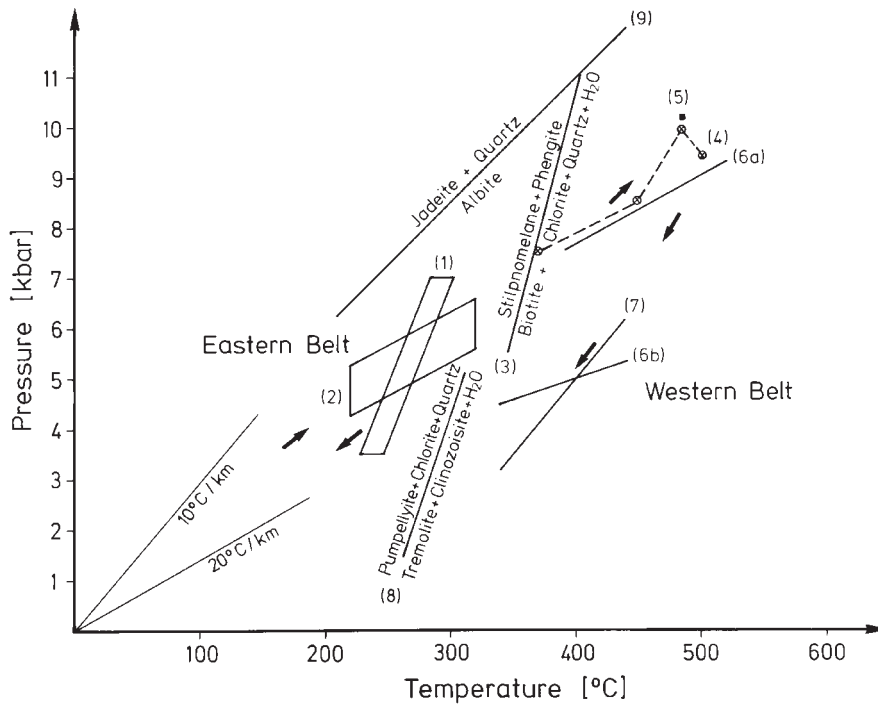
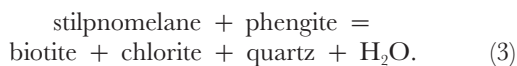


**Fig. 7.** Petrogenetic grid and *P-T* paths for the Chonos Metamorphic Complex; *P-T* conditions in the Eastern belt are marked by reaction bands (1) and (2) referring to reactions of equal index number in the text. Reaction (3) is according to Massonne & Szpurka (1997). *P-T* evolution in the Western belt is given by numbers (4)–(8): (4) marks the four-stage calculated *P-T* path for sample 96CH-113 related to garnet growth (*T*3, *P*1 of Table 6), (5) the maximum *P-T* conditions for sample 96CH-113 calculated including white mica (*T*5, *P*3 of Table 6). Reaction (6a) marks the calculated maximum pressure conditions for garnet-free sample 96CH-71. Retrograde conditions after garnet growth are given by the reactions (6b) and (7) for sample 96CH-113 (*T*6, *P*4 of Table 6). Pumpellyite ‘out’ reaction (8) is according to Evans (1990), the albite breakdown curve (9) according to Holland (1980).

Peak temperature conditions reached in metabasites and meta-ironstones are indicated by the growth of biotite in Fe-rich rocks, such as the stilpnomelane-bearing meta-ironstones 96CH-67 and 96CH-71 and the greenschist Fo96-14. These maximum temperatures were reached after *D*<sub>2</sub> deformation, because biotite growth is always oblique to *S*<sub>2</sub>.

Massonne & Szpurka (1997) determined stilpnomelane breakdown to biotite in the KFLASH system in the presence of phengite and quartz at about 350–400°C and 6–10 kbar by the reaction



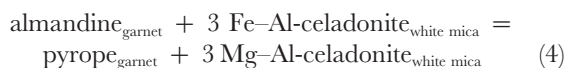
The assemblage stilpnomelane–phengite–quartz–chlorite, however, still exists in meta-ironstone Fo96-41. This rock also contains primary actinolite and chlorite and hence it represents the lowest peak temperature in the Western belt. On the other hand, the assemblages biotite–chlorite–stilpnomelane–quartz in samples 96CH-71 and 96CH-67 and biotite–chlorite–quartz in sample Fo96-14, but also stilpnomelane–quartz in numerous meta-ironstones, are compatible with the overstepping of reaction (3). This conclusion is also supported by the

common assemblage white mica–biotite–chlorite–quartz, observed by Miller (1979). This indicates that in most parts of the Western belt maximum temperatures must have exceeded 400°C.

It should be noted here that stilpnomelane compositions do not show any significant variation between and within the two belts. Moreover, it is remarkable that *X*<sub>Fe</sub>, although variable among samples, hardly varies within a single sample. The generally random orientation of this mineral is also remarkable. The interlayer occupation of stilpnomelane varies in all samples unsystematically between 0.2 and 0.8; this might be an alteration phenomenon.

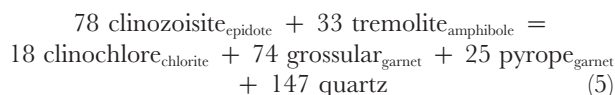
The garnet-bearing metabasites 96CH-113 and Fo96-39 are the only metabasite samples containing garnet. The observed oscillatory zoning pattern of garnet combined with specific inclusions of chlorite, epidote and amphibole that can be assigned to each garnet zone representing a transient compositional domain provides a unique opportunity to reconstruct a prograde *P-T* path from a set of continuous multivariant reactions. This is defined by four successive stages during growth of garnet (Fig. 3) with the correlation of mineral compositions explained above (Table 6). Using conventional ther-

mometry by amphibole–garnet Mg–Fe exchange, the best results are provided by the approach of Graham & Powell (1984), which takes the influence of the grossular component in garnet solid solutions into account. Resulting temperatures increase irregularly from garnet growth stages 2a to 2d (Table 6; *T1*) from 339°C to 407°C. Significantly higher temperatures for stage 2d at 551°C (Table 6; *T2*) result when the Fe–Mg exchange reaction



between garnet and phengite is thermodynamically calculated.

Additional *P–T* data were calculated by intersection of the *P–T* position of the water-independent multivariant equilibrium



and six further ones also involving albite and the glaucophane component of the amphiboles (Fig. 8). Results show increasing temperatures and pressures from 375°C and 7.5 kbar to 507°C and 9.4 kbar (Table 6, *T3*, *P1*; Fig. 7, path 4). Reaction (5) will shift towards temperatures about 40°C lower when the garnet mixing model of Berman (1990) is applied, which provides less adaptation of the influence of the high spessartine concentration of the garnet (Table 6, *T4*, *P2*).

The oscillatory zoning that was observed only in the element distribution map of garnet possibly results from a variation of the slope of the *P–T* path, within the error of above presented values. During non-uniform pressure and temperature increase (e.g. by variation in subduction velocity) the contribution of different garnet-producing reactions to the growth of garnet will vary, when they have markedly different slopes. Such different continuous reactions may be either Ca–Mg-garnet forming reactions such as reaction (4) or Fe–Mg exchange reactions. Such an explanation for oscillatory zoning has been advocated by Schumacher *et al.* (1999).

Although it is difficult to relate compositions of white mica from the same rock to the garnet zones, compositions with highest Si contents could be correlated with the rim stage of garnet, whereas low-Si rim compositions in mica probably correspond to retrograde stages. The following multivariant equilibrium provides a good barometer to test this assumption:

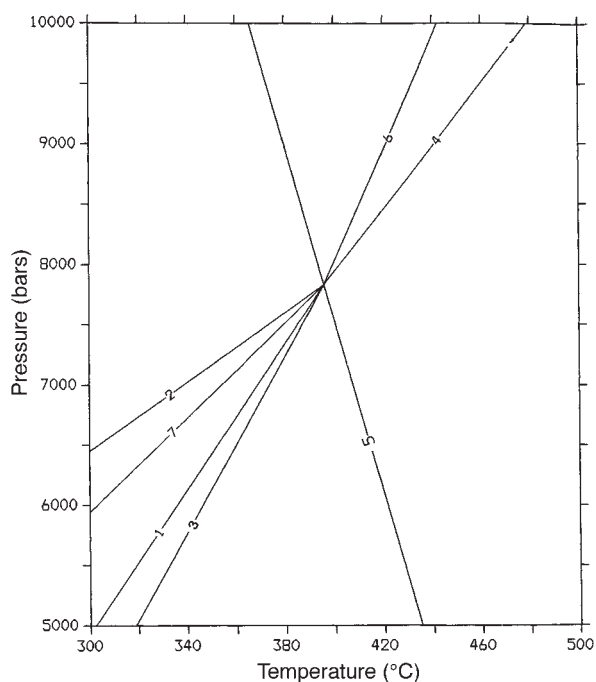
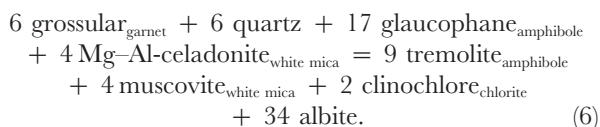


**Fig. 8.** *P–T* estimate using the Ge0-Calc software for stages of garnet growth in sample 96CH-113. (For explanation see text.) Numbers 1–7 refer to the following water-independent multivariant reactions:

- (1)  $37 \text{Gl} + 10 \text{Czo} + 21 \text{Qz} = 74 \text{Ab} + 8 \text{Chl} + 7 \text{Py} + 10 \text{Tr}$ ;
- (2)  $8 \text{Gr} + \text{Py} + 21 \text{Qz} + 9 \text{Gl} = 6 \text{Czo} + 6 \text{Tr} + 18 \text{Ab}$ ;
- (3)  $7 \text{Gl} + 4 \text{Czo} = 14 \text{Ab} + 2 \text{Chl} + 2 \text{Gr} + 2 \text{Py} + \text{Tr}$ ;
- (4)  $39 \text{Gl} + 42 \text{Qz} + 10 \text{Gr} = 78 \text{Ab} + 6 \text{Chl} + 4 \text{Py} + \text{Tr}$ ;
- (5)  $18 \text{Chl} + 74 \text{Gr} + 25 \text{Py} + 147 \text{Qz} = 78 \text{Czo} + 33 \text{Tr}$ ;
- (6)  $30 \text{Czo} + 33 \text{Gl} = 21 \text{Qz} + 13 \text{Py} + 20 \text{Gr} + 12 \text{Chl} + 66 \text{Ab}$ ;
- (7)  $14 \text{Gr} + 42 \text{Qz} + 25 \text{Gl} = 8 \text{Czo} + 13 \text{Tr} + 2 \text{Chl} + 50 \text{Ab}$ .

Abbreviations for the components in solid solution are: Ab, albite; Chl, clinocllore; Czo, clinozoisite; Gl, glaucophane; Gr, grossular; Py, pyrope; Qz, quartz.

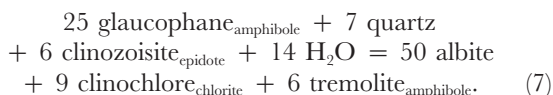
Intersection with reaction (5) and four further multivariant equilibria involving white mica components results in maximum *P–T* conditions at 10.2 kbar and 485°C and during the final stage of garnet growth (point 5 in Fig. 7; *T5*, *P3* in Table 6) in agreement with the above derived peak *P–T* conditions.

On the other hand, potassic white mica rim compositions relatively poor in Si would indicate unreasonably high temperatures on applying thermometer (4). Therefore decreasing Si contents towards the rims of the white micas are interpreted as the result of retrograde reactions. This is also assumed for decreasing Al content in the rim of matrix epidote and increasing tremolite component toward the rim of matrix amphibole (Table 6, stages 3 and 4). These compositional features are compatible with decreasing temperature and pressure.

The garnet also provides strong indication on the timing of the development of the foliations *S*<sub>1</sub> and *S*<sub>2</sub>.

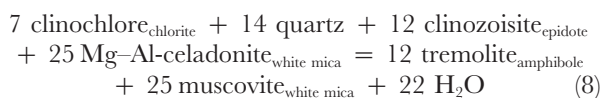
During late prograde growth garnet overgrew the clearly prograde  $S_1$ , whereas development of the  $S_2$  foliation started during late growth of garnet as a result of deflection of  $S_1$  at the outer zone of garnets (see above). It evidently formed during attainment of maximum pressures and presumably proceeded during the early decompression path.

The following multivariant reaction provides geobarometric information for metabasites that do not contain garnet:



Because water activity was possibly below unity, only maximum pressure can be determined. The *P-T* position of this reaction calculated for core compositions in sample 96CH-71 (Fig. 7, line 6a) is close to the maximum pressure conditions calculated for the garnet-bearing metabasite.

The same reaction can also be used to calculate retrograde conditions for the garnet-bearing sample 96CH-113 (stage 3 in Table 6; line 6b in Fig. 7). It intersects with the following reaction typical for greenschist facies conditions, which involves white mica:



and with three other reactions involving also the glaucophane component of amphibole. The corresponding *P-T* point was calculated with a white mica rim composition showing the lowest Si content (white mica II) and an amphibole rim composition (amphibole IV; Tables 1–6) as well as with a clearly retrograde chlorite and epidote. The result of 400°C and 5 kbar contributes to define the retrograde *P-T* path ( $T_6$ ,  $P_4$  in Table 6).

Cores of some amphibole with high tremolite content (amphibole I) and of epidote with high clinozoisite content (epidote I) in sample 96CH-113 also represent low-temperature–low-pressure conditions from a preserved prograde stage. Prograde temperature increase is documented by the trend of decreasing Si contents and  $X_{\text{Mg}}$  in the hornblends of the common basic rocks (Fig. 4; samples 96CH-110 and Fo96-35). On the other hand, decrease of the glaucophane component and increase of tremolite component is observed towards the rims of amphiboles in samples 96CH-113, Fo96-14 and 96CH-71, indicating retrograde cooling and pressure release. In both cases, the respective amphiboles are oriented parallel to the  $S_2$  foliation.

#### *Metapsammopelites*

The metapsammopelitic rocks of the Western belt show the uniform assemblage white mica–chlorite–quartz.

Miller (1979) also described late strain-free formation of biotite coexisting with white mica and chlorite in local metapelitic assemblages, which might be due to Al-poorer whole-rock compositions. Both assemblages are compatible with the maximum temperature range derived from the metabasites.

Although a well-tested thermometer could not be applied to the metapelitic assemblages, white mica compositions provide information on the pressure of their formation. White micas in the metapelites of the CMC are generally phengites. The range of Si contents between 3.2 and 3.4 p.f.u. is compatible with the *P-T* evolution recorded above. Thus, the highest-pressure conditions determined above seem to be randomly spread in the Western belt. The retrograde *P-T* path resulted in a decrease of the Si contents of phengite as observed at their rim. In one sample only low Si contents (96CH-103) are recorded. Deviating conditions at this locality with respect to other rocks of the Western belt are also indicated by actinolites in meta-ironstone sample Fo96-41 and the stability of stilpnomelane + phengite.

$X_{\text{Mg}}$  of the white micas does not show any variation in studied samples from the Western belt, in contrast to sample Fo96-15 of the Eastern belt, which shows a prograde relationship of Si content and  $X_{\text{Mg}}$ . This might indicate a nearly isothermal decompression experienced by these rocks.

## DISCUSSION AND CONCLUSION

Mineral chemical analyses and thermobarometric evaluation in various rock types available from the CMC showed that, in general, prograde as well as retrograde metamorphism can be demonstrated, during which equilibration was achieved in local small-scale domains within single rocks under different conditions. As a result of the specific reaction history of different rock types the degree of equilibration under specific conditions varies. Prograde information comes mainly from growth zoning of some solid solutions that were generally oriented by penetrative deformation, whereas retrograde strain-free imprints depend on the local availability of external hydrous fluid influx.

Maximum *P-T* conditions recorded are 4.5–6 kbar and 250–280°C for the Eastern belt and 8–10 kbar and 380–550°C for the Western belt. This confirms widespread high-pressure–low-temperature equilibration as a result of low geotherms between 10 and 20°C/km. Such conditions can develop in accretionary prisms, where subduction is relatively slow. The limits of the pumpellyite–actinolite facies, and the greenschist and albite–epidote amphibolite facies transitions with the epidote–blueschist facies were reached. Mineral compositions of amphibole and white mica in greenschists

and metasediments of the Eastern belt are very similar to those of very low grade rocks of the Sanbagawa belt, Japan (Banno & Sakai, 1989; Banno, 1998), whereas those in the Western belt are comparable with those of the Catalina Schist terrane, California (Sorensen, 1986). In both cases, also, high pressure and low-temperature conditions were assumed. Thus both the Western and Eastern belt formed part of a subduction system.

Formation of dominant foliations in both belts correlates with maximum pressure and temperature attained, because of orientation of phases that indicate maximum  $P$ - $T$  conditions. This indicates that both  $S_1$  and  $S_2$  represent deformation episodes that were related to the process of accretion during formation of the subduction complex. However, in the Western belt growth relationships demonstrated by rare garnet showed that  $S_1$  was a prograde deformation feature, whereas  $S_2$  commenced at maximum pressure. Presumably, there was a time of low differential stress during the latest stage of burial. This was advocated by Stöckhert *et al.* (1997), on the basis of a thorough study of similar relationships in a palaeosubduction zone in the Eastern Alps, and was interpreted as transition from the downgoing to the overriding plate in the zone of basal accretion.

On the other hand, retrograde minerals generally grew or continued growing strain free. Retrograde deformation seems to be confined to kinking or brittle structures. The extent of retrograde overprint, which indicates an overall trend of slight cooling with decompression, varies strongly. Another retrograde phenomenon that is widespread and conspicuous is the growth of albite porphyroblasts as the latest mineral in both metapsammopelites and in greenschists, generally after formation of  $S_2$ . The appearance of albite porphyroblasts is uniform throughout the Western belt. We assume that the albite porphyroblasts may have formed by a process similar to that described by Jamieson & O'Beirne-Ryan (1991). Those workers pointed out that this phenomenon may be due to ionic reactions taking place upon pressure release and cooling, during which the albite stability field expands relative to white mica. In any case, the widespread appearance of the phenomenon throughout the Western belt (Miller, 1978; Godoy *et al.*, 1984; Davidson *et al.*, 1987) and the variable local intensity of albite porphyroblastesis imply the presence of a hydrous fluid during exhumation. This is also indicated by the extensive retrograde growth of hydrous low-grade assemblages, and may be related to continuing underplating of prograde dehydrating sediments. Slight cooling during decompression as evidenced by the  $P$ - $T$  path of the Western belt is also an indicator of continuing accretion of cooler rocks below the Western belt during its uplift.

Although evidently formed within the same overall geotectonic environment, the two belts show important differences:

(1) the relative abundance of lithologies is different, e.g. greenschists are mainly confined to the Western belt, where rocks of continental and oceanic provenance are thoroughly mixed;

(2) the preservation of primary structures and stratal continuity occurs only in the Eastern belt except for local zones of 'broken formations', in contrast to the Western belt, where transposition parallel to a  $S_2$  foliation is complete and an earlier  $S_1$  developed early during the prograde  $P$ - $T$  path;

(3) as shown above, maximum temperatures and pressures attained show a  $P$ - $T$  gap between the two belts, i.e. penetrative deformational imprint occurred at very different depths in the two belts.

Because samples of both belts showing different  $P$ - $T$  conditions were taken close to their border (Fig. 1), a gradual transition as suggested by Davidson *et al.* (1987) seems to be unlikely. Moreover, the polarity of the metamorphic facies distribution is inverse compared with the classic concept of Ernst (1975) proposed for many other circum-Pacific subduction complexes. Godoy *et al.* (1984) and Davidson *et al.* (1987) supposed very different ages of formation of the two belts, partly based on the different Rb-Sr whole-rock isochron ages. This becomes obvious when the mode of formation of both belts is taken into consideration: whereas rocks of the Western belt have characteristics of basal accretion at depth, all features of the Eastern belt point to an origin at a high level by frontal accretion. Hence the best explanation of the regional situation would be a phase of rapid prograde growth of the accretionary prism towards the west followed by a destructive phase of shortening toward the east involving tectonic erosion and thickening in the west, which caused uplift of the deep-seated Western series.

The absence of very low grade metamorphic rocks to the west of the Western belt as would be expected in a model with subduction from western directions can be explained by tectonic erosion. Such a process is generally assumed to be responsible for migration of the Mesozoic magmatic arcs in Northern Chile, which cannot be explained otherwise by the migration of the subduction zone (e.g. Reutter *et al.*, 1988). A mechanism for tectonic erosion can be subduction of an oceanic ridge. This was shown by Bangs & Cande (1997) for the recent South Chilean subduction zone, where a recent accretionary wedge is missing above the currently subducting Chile rise. Moreover, ridge subduction was advocated by Trouw *et al.* (1998) as a principal cause of exhumation and preservation of a deep-seated palaeosubduction complex in the South Shetland Islands-Antarctica. This mechanism seems to be important for exhumation of HP-LT rocks, which is strongly diachronous and discontinuous in space and time along the Pacific margin of Central and Southern Chile (Hervé, 1988).

Although important geochronological and kinematic information is still lacking, the most likely explanation for the Eastern belt is that it formed not only a less deep subducted part, but also a transitional part toward the backstop system of the accretionary prism at a late stage of its development. The very low grade metasediments also occupy a very large area east of the CMC on the mainland east of Puerto Aisen (Fig. 1). As in the Eastern belt, intercalations of metabasites are rare or absent (Hervé, 1988).

Godoy *et al.* (1984) and Davidson *et al.* (1987) suggested juxtaposition of the two belts during the  $D_2$  event. However, as was shown above,  $D_2$  is rather a deformational imprint during maximum burial and not related to the main part of exhumation. Exhumation, by contrast, must be related to the event that produced the final boundary between the belts. Apart from the marked differences in metamorphic conditions occurring within a relatively short distance, especially in the northern part of the area studied, the contact, as far as it is mapped at present, always cuts former ductile structures at a low to moderate angle, as shown clearly by the detailed mapping of a portion of the CMC by Garrido (1987) and Hormazábal (1991). This points towards a discrete upper-crustal boundary, along which the final juxtaposition of the belts took place. The boundary might also be, at least partly, a fault system related to the long-lived mainly Cenozoic intra-arc Liquiñe Ofqui fault system (Cembrano *et al.*, 1996). Subsidiary faults cutting the CMC were assumed by Cembrano *et al.* (1996) to have caused anticlockwise block rotations during oblique subduction of the Nazca plate.

## ACKNOWLEDGEMENTS

This research was supported by Catedra Presidencial en Ciencias and FONDECYT Project 1950/544 to F.H. and by the German–Chilean BMBF-CONICYT co-operation project ‘High pressure metamorphic rocks in Chile’. V. Munoz and C. Pimperev participated in the 1996 field leg. H.-J. Bernhardt kindly supported microprobe work in Bochum, as did B. Schulz-Dobrick in Mainz. Comments by T. Hirajima and F. Lucassen on an earlier version of the manuscript are gratefully acknowledged, as well as advice by H.-J. Gursky on the metacherts. Special thanks are due to R. Trouw and an anonymous reviewer for valuable reviews, as well as to S. L. Harley for editorial handling. We enjoyed perfect logistic support in the field by the crew of CONAF’s boat *Petrel*. This paper is a contribution to IGCP 436 ‘Pacific Gondwana Margin’.

## REFERENCES

- Aguirre, L., Hervé, F. & Godoy, E. (1972). Distribution of metamorphic facies in Chile: an outline. *Krystallinikum* **9**, 7–19.
- Bangs, N. L. & Cande, S. C. (1997). The episodic development of a convergent margin inferred from structures and processes along the Southern Chile margin. *Tectonics* **16**, 489–503.
- Banno, S. (1998). Pumpellyite–actinolite facies of the Sanbagawa metamorphism. *Journal of Metamorphic Geology* **16**, 117–128.
- Banno, S. & Sakai, C. (1989). Geology and metamorphic evolution of the Sanbagawa belt, Japan. In: Daly, S., Cliff, R. A. & Yardley, B. W. D. (eds) *Evolution of Metamorphic Belts*. Geological Society, London, *Special Publication* **43**, 519–531.
- Berman, R. G. (1988). Internally-consistent thermodynamic data for minerals in the system  $\text{Na}_2\text{O}-\text{K}_2\text{O}-\text{CaO}-\text{MgO}-\text{FeO}-\text{Fe}_2\text{O}_3-\text{Al}_2\text{O}_3-\text{SiO}_2-\text{TiO}_2-\text{H}_2\text{O}-\text{CO}_2$ . *Journal of Petrology* **29**, 445–522.
- Berman, R. G. (1990). Mixing properties of Ca–Mg–Fe–Mn garnets. *American Mineralogist* **75**, 328–344.
- Brown, T. H., Berman, R. G. & Perkins, E. H. (1989). GeO–Calc: software package for calculation and display of pressure–temperature–composition phase diagrams using an IBM or compatible personal computer. *Computers and Geosciences* **14**, 279–289.
- Cembrano, J., Hervé, F. & Lavenu, A. (1996). The Liquiñe Ofqui fault zone: a long-lived intra-arc fault system in southern Chile. *Tectonophysics* **259**, 55–66.
- Davidson, J., Mpodozis, C., Godoy, E., Hervé, F., Pankhurst, R. J. & Brook, M. (1987). Late Paleozoic accretionary complexes on the Gondwana margin of southern Chile: evidence from the Chonos Archipelago. In: McKenzie, G. D. (ed.) *Gondwana Six: Structure, Tectonics and Geophysics*. Geophysical Monograph, American Geophysical Union **40**, 221–227.
- Ernst, W. G. (1975). Systematics of large-scale tectonics and age progressions in Alpine and Circum-Pacific blueschist belts. *Tectonophysics* **26**, 229–246.
- Evans, B. W. (1990). Phase relations of epidote blueschists. *Lithos* **25**, 3–23.
- Fang, Z., Boucot, A., Covacevich, V. & Hervé, F. (1998). Discovery of Late Triassic fossils in the Chonos Metamorphic Complex, Southern Chile. *Revista Geológica de Chile* **25**, 165–173.
- Garrido, I. (1987). Geología y petrología de Isla Teresa, Archipiélago de los Chonos, Aysén. M.Sc. thesis, Universidad de Chile, Santiago, 127 pp.
- Godoy, E., Hervé, F., Mpodozis, C. & Davidson, J. (1984). Deformación polifásica y metamorfismo progresivo en el basamento de Archipiélago de los Chonos, Aysén, Chile. *Actas IX Congreso Geológico Argentino, Bariloche* **4**, 211–232.
- Graham, C. M. & Powell, R. (1984). A garnet–hornblende geothermometer and application to the Peloma Schist, southern California. *Journal of Metamorphic Geology* **2**, 13–32.
- Hervé, F. (1988a). Late Paleozoic subduction and accretion in Southern Chile. *Episodes* **11**, 183–188.
- Hervé, F. (1988b). Late Triassic rocks in the subduction complex of Aysén, Southern Chile. *Journal of African Earth Sciences, Special Abstract Volume, Gondwana 10: Event Stratigraphy of Gondwana* **27**, 224.
- Hervé, F., Mpodozis, C., Davidson, J. & Godoy, E. (1981). Observaciones estructurales y petrográficas en el basamento metamórfico del archipiélago de los Chonos, entre el Canal King y el Canal Ninualac, Aisen. *Revista Geológica de Chile* **13–14**, 3–16.
- Hervé, F., Godoy, E., Garrido, I., Hormazábal, L. & Brook, M. (1988). Geocronología y condiciones de metamorfismo del complejo de subducción del archipiélago de los Chonos. *Actas V Congreso Geológico Chileno, Santiago* **2**, E157–E173.

- Hervé, F., Greene, F. & Pankhurst, R. J. (1994). Metamorphosed fragments of oceanic crust in the Upper Paleozoic Chonos accretionary complex, Southern Chile. *Journal of South American Earth Sciences* **7**, 7–14.
- Hervé, F., Larrondo, P., Pankhurst, R. J. & Haller, M. (1997). El granito Peninsula Gallegos–Isla Clemente, Aysen: Un ejemplo de intrusión cercana a la fosa del Cretácico superior? *Actas VIII Congreso Geológico Chileno, Antofagasta* **3**, 1645–1649.
- Holland, T. J. B. (1980). The reaction albite = jadeite + quartz determined experimentally in the range 600–1200°C. *American Mineralogist* **65**, 129–134.
- Hormazábal, L. (1991). Geología del basamento metamórfico del grupo Isote Smith e islas aldanas, entre los 45°–45°15' Latitud Sur, Aysen, Chile. M.Sc. thesis, Universidad de Chile, Santiago, 97 pp.
- Jamieson, R. A. & O'Beirne-Ryan, A. M. (1991). Decompression induced growth of albite porphyroblasts, Fleur de Lys Supergroup, western Newfoundland. *Journal of Metamorphic Geology* **9**, 433–439.
- Leake, B. E. (1978). Nomenclature of amphiboles. *Canadian Mineralogist* **16**, 501–520.
- Massonne, H.-J. (1995a). *P–T* evolution of metovolcanics from the southern Taunus mountains. In: Dallmeyer, R. D., Franke, W. & Weber, K. (eds) *Pre-Permian Geology of Central and Eastern Europe*. Berlin: Springer, pp. 132–137.
- Massonne, H.-J. (1995b). Experimental and petrogenetic study of UHPM. In: Coleman, R. G. & Wang, X. (eds) *Ultrahigh Pressure Metamorphism*. Cambridge: Cambridge University Press, pp. 33–95.
- Massonne, H.-J. & Szpurka, Z. (1997). Thermodynamic properties of white micas on the basis of high-pressure experiments in the systems  $K_2O$ – $MgO$ – $Al_2O_3$ – $SiO_2$ – $H_2O$  and  $K_2O$ – $FeO$ – $Al_2O_3$ – $SiO_2$ – $H_2O$ . *Lithos* **41**, 229–250.
- Massonne, H.-J., Hervé, F., Munoz, V. & Willner, A. P. (1996). New petrological results on high-pressure, low-temperature metamorphism of the Upper Paleozoic basement of Central Chile. *Extended Abstracts, 3rd International Symposium on Andean Geodynamics, St Malo*, pp. 783–785.
- Miller, H. (1979). Das Grundgebirge der Anden im Chonos-Archipel, Region Aisén, Chile. *Geologische Rundschau* **68**, 428–456.
- Pankhurst, R. J. & Hervé, F. (1994). Granitoid age distribution and emplacement control in the North Patagonian batholith in Aysén, Southern Chile. *Actas VII Congreso Geológico Chileno* **2**, 1409–1413.
- Reutter, K.-J., Giese, P., Götze, H.-J., Scheuber, E., Schwab, K., Schwarz, G. & Wigger, P. (1988). Structures and crustal development of the Central Andes between 21° and 25°S. In: Bahlburg, H., Breikreuz, Ch. & Giese, P. (eds) *The Southern Central Andes*. Berlin: Springer, pp. 231–261.
- Schumacher, R., Rötzler, K. & Maresch, W. V. (1999). Subtle oscillatory zoning in garnet from regional metamorphic phyllites and mica schists, Western Erzgebirge, Germany. *Canadian Mineralogist* **37**, 381–402.
- Sorensen, S. S. (1986). Petrologic and geochemical comparison of the blueschist and greenschist units of the Catalina schists, southern California. *Geological Society of America, Memoir* **164**, 59–75.
- Spear, F. S. (1980). NaSi ↔ CaAl exchange equilibrium between plagioclase and amphibole. *Contributions to Mineralogy and Petrology* **72**, 33–41.
- Stöckhert, B., Massonne, H.-J. & Nowlan, E. U. (1997). Low differential stress during high-pressure metamorphism: the microstructural record of a metapelite from the Eclogite Zone, Tauern Window, Eastern Alps. *Lithos* **41**, 103–118.
- Trouw, R. A. J., Simoes, L. S. A. & Valladares, C. S. (1998). Metamorphic evolution of a subduction complex, South Shetland Islands, Antarctica. *Journal of Metamorphic Geology* **16**, 475–490.